Salt Heater Test (FY19)

Spent Fuel and Waste Disposition

Prepared for
US Department of Energy
Spent Fuel and Waste Science and Technology

Sandia National Laboratories
Melissa Mills, Kris Kuhlman, Ed Matteo, Courtney Herrick, Martin Nemer, Jason Heath, Yongliang Xiong, Carlos Lopez

Los Alamos National Laboratory
Phil Stauffer, Hakim Boukhalfa, Eric Guiltinan, Thom Rahn, Doug Weaver, Brian Dozier, Shawn Otto

Lawrence Berkeley National Laboratory
Jonny Rutqvist, Yuxin Wu, Mengsu Hu

National Energy Technology Laboratory
Dustin Crandall

August 30, 2019
M3SF-19SN01030303, SAND2019-10240 R

DISCLAIMER

This information was prepared as an account of work sponsored by an agency of the U.S. Government. Neither the U.S. Government nor any agency thereof, nor any of their employees, makes any warranty, expressed or implied, or assumes any legal liability or responsibility for the accuracy, completeness, or usefulness, of any information, apparatus, product, or process disclosed, or represents that its use would not infringe privately owned rights. References herein to any specific commercial product, process, or service by trade name, trade mark, manufacturer, or otherwise, does not necessarily constitute or imply its endorsement, recommendation, or favoring by the U.S. Government or any agency thereof. The views and opinions of authors expressed herein do not necessarily state or reflect those of the U.S. Government or any agency thereof.

Sandia National Laboratories is a multimission laboratory managed and operated by National Technology and Engineering Solutions of Sandia LLC, a wholly owned subsidiary of Honeywell International Inc. for the U.S. Department of Energy's National Nuclear Security Administration under contract DE-NA0003525.

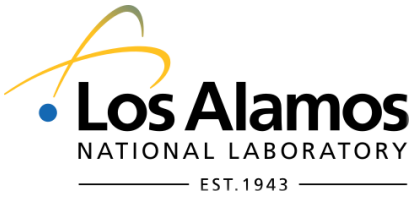

VERSION INFO

This report summarizes the 2019 fiscal year (FY19) status of the borehole heater test in salt funded by the US Department of Energy Office of Nuclear Energy (DOE-NE) Spent Fuel and Waste Science & Technology (SFWST) campaign. This report satisfies SFWST level-three milestone report M3SF-19SN010303033. This report is an update of the April 2019 level-two milestone report M2SF-19SN010303031 to reflect the nearly complete as-built status of the borehole heater test.

Revision 0	April 11	DOE-NE Concurrence Draft	SNL Programmatic Tracking Number: 948458 M2SF-19SN010303031
Revision 1	April 30	Public Release	SAND2019-4814 R
Revision 2	August 30	Public Release	M3SF-19SN010303033; SAND2019-10240 R

ACKNOWLEDGEMENTS

The authors include a team across several national laboratories. At Sandia National Laboratories (SNL) the team includes Kris Kuhlman, Melissa Mills, Courtney Herrick, Ed Matteo, Martin Nemer, Yongliang Xiong, Carlos Lopez, and Jason Heath. At Los Alamos National Laboratory (LANL) the team includes Phil Stauffer, Hakim Boukhalfa, Doug Ware, Eric Guiltinan, and Thom Rahn. At LANL Carlsbad, representing the Waste Isolation Pilot Plant (WIPP) Test Coordination Office (TCO), are Doug Weaver, Brian Dozier, and Shawn Otto. At Lawrence Berkeley National Laboratory (LBNL) the team includes Jonny Rutqvist, Yuxin Wu, and Mengsu Hu.

The authors thank Dustin Crandall from National Energy Technology Laboratory (NETL) for providing preliminary imaging and characterization results from the salt cores. We also acknowledge the assistance and support of the WIPP underground facilities personnel, who make the implementation in the underground possible, and support of the DOE Office of Environmental Management (DOE-EM) Carlsbad Field Office (CBFO) chief scientist, George Basabilvaso. The authors acknowledge Ernie Hardin and K-Won Chang (SNL) for reviewing versions of this document.

CONTENTS

LIST OF FIGURES

LIST OF TABLES

ACRONYMS

AE	acoustic emissions (also BATS AE boreholes)
BATS	brine availability test in salt
CBFO	Carlsbad field office (DOE-EM WIPP office)
CPU	central processing unit
CRDS	cavity ring-down spectrometer
CT	computed tomography
D	BATS source borehole
DAS	data acquisition system
DOE	Department of Energy
DOE-EM	DOE Office of Environmental Management
DOE-NE	DOE Office of Nuclear Energy
DRZ	disturbed rock zone
DSS	distributed strain sensing
DTS	distributed temperature sensing
E	BATS ERT boreholes
ERT	electrical resistivity tomography
F	BATS fiber boreholes
FY	fiscal year (October-September)
GRS	Gesellschaft für Anlagen- und Reaktorsicherheit
GWB	G-seep WIPP brine
HP	BATS heater/packer borehole
ICP-MS	inductively coupled plasma mass spectrometry
LANL	Los Alamos National Laboratory
LBNL	Lawrence Berkeley National Laboratory
LVDT	linear variable differential transformer
MB-139	marker bed 139 (WIPP stratigraphic unit) – also MB-140
MU-0	map unit 0 (WIPP stratigraphic unit) – also MU-1 through MU-6
NEMA	national electrical manufacturer association
NETL	National Energy Technology Laboratory
NQA	nuclear quality assurance
NWP	Nuclear Waste Partnership
OMB	orange marker band
PA	performance assessment
PEEK	polyetheretherketone thermoplastic
POM	polyoxymethylene thermoplastic
PVC	polyvinyl chloride plastic
R&D	research and development
RH	relative humidity
SDI	Salt Disposal Investigations (proposed CBFO program)
SEM	scanning electron microscopy
SFWST	Spent Fuel & Waste Science & Technology (DOE-NE program)
SNL	Sandia National Laboratories
SL	BATS seal borehole
SM	BATS liquid sampling borehole
SRS	Stanford Research Systems
STP	standard temperature and pressure
T	BATS thermocouple boreholes
TCO	WIPP Test Coordination Office
TGA	thermogravimetric analysis
THMC	thermal-hydrological-mechanical-chemical (also THM & THC)
UHP	ultra-high purity
US	United States
WIPP	Waste Isolation Pilot Plant (DOE-EM site)
XRD	X-ray diffraction
XRF	X-ray fluorescence

This page is intentionally left blank.

SALT HEATER TEST (FY19)

This report discusses the fiscal year 2019 (FY19) design, implementation, and preliminary data interpretation plan for a set of borehole heater tests call the brine availability tests in salt (BATS), which is funded by the DOE Office of Nuclear Energy (DOE-NE) at the Waste Isolation Pilot Plant (WIPP), a DOE Office of Environmental Management (DOE-EM) site.

The organization of BATS is outlined in *Project Plan: Salt In-Situ Heater Test* (SNL, 2018). An early design of the field test is laid out in Kuhlman et al. (2017), including extensive references to previous field tests, which illustrates aspects of the present test. The previous test plan by Stauffer et al. (2015) places BATS in the context of a multi-year testing strategy, which involves tests of multiple scales and processes, eventually culminating in a drift-scale disposal demonstration. This level-3 milestone report is an update of a level-2 milestone report from April 2019 by the same name. The update adds as-built details of the heater test, which at the time of writing (August 2019) is near complete implementation.

1. Background and Test Overview

The main focus of the BATS field test is on brine availability in salt. These field tests are the first part of a wider systematic field investigation campaign to improve the existing long-term repository safety case for disposal of heat-generating radioactive waste in salt. Future tests will explore other aspects of the safety case, as justified by their impacts on long-term performance. These first tests seek to better understand how much brine can flow into an excavation (e.g., borehole or room) in salt. Brine availability is important to the long-term repository safety case for radioactive waste disposal in salt (Kuhlman & Sevougian, 2013) because: 1) brine can facilitate transport of radionuclides off-site, 2) brine can corrode metallic and glass waste forms and metal waste packages, 3) chloride in brine can reduce waste package criticality concerns, and 4) accumulated brine in an excavation can provide back-pressure that resists long-term creep closure of a repository excavation. In a generic salt repository for “hot” radioactive waste (i.e., above brine boiling temperature at the waste package surface) an area around the waste packages will dry out when water vapor is driven away. Bound water in hydrous evaporite minerals can become mobile upon heating, while thermal expansion of intergranular brine drives flow towards lower-pressure regions. Additionally, a small-scale short-term heat pipe convection process can set up in the partially saturated region around the waste (Jordan et al., 2015) driving salt precipitation near the waste package and salt dissolution where steam condenses. In the longer-term, creep closure further reconsolidates backfill, closes gaps around waste packages, and heals the access-drift disturbed rock zone (DRZ) to create a relatively dry, intact, low-permeability zone around the waste packages (Blanco-Martín et al., 2018). Knowledge of brine availability and brine composition facilitates understanding the amount and distribution of brine that flows to an excavation, as well as the long-term behavior of brine around waste packages that affects transport (i.e., brine-radionuclide interactions).

In undisturbed salt disposal systems, the far-field ultra-low permeability and porosity of the salt (Beauheim & Roberts, 2002) provides the primary natural barrier to contain radioactive waste over performance assessment (PA) relevant time scales (10^4 to 10^6 years). However, near-field conditions (e.g., pressures, saturations, compositions) and processes (e.g., brine and gas flow, salt creep) will impact releases in an off-normal disturbed scenario and are the initial conditions for a long-term PA simulation. BATS is focused on the quantification of inflow rates and brine composition in the near-field (at scales of cm to m from the heat source) with the aim to improve: 1) our understanding and observations of coupled thermal-hydrological-mechanical-chemical (THMC) processes affecting prediction of near-field conditions; 2) conceptual models of near-field behavior that inform the safety case; and 3) the numerical models, constitutive relationships, and parameterizations that are implemented in PA models.

Brine availability in a salt repository depends on both the distribution of water in the formation and the flow and transport properties of the DRZ surrounding an excavation (Kuhlman & Malama, 2013). The distribution of brine and bound water in the salt formation (i.e., intragranular brine, intergranular brine,

and hydrous minerals) includes the distribution of water in both the liquid and gas phases before and during the test. The primary DRZ property of interest for the test is the distribution and evolution of damage (i.e., porosity and permeability of the matrix and induced fractures) around the access drift and test boreholes, which will likely provide the primary path for flow towards the test boreholes.

The first phase of the BATS test comprises two initial horizontal borehole heater tests to be conducted in the Salt Disposal Investigation (SDI) area drifts (on the south side of N-940 west of E-540; see Figure 1) of WIPP. Two arrays of horizontal boreholes have been drilled (heated and unheated arrays), each following the pattern shown in Figure 2. Follow-on borehole tests may be designed using similar arrangements to what is presented here but capitalizing on lessons learned from this first phase of testing.

One test array will be heated (heater in central HP borehole) and the other pattern will be a similar layout, but unheated. Each array will be configured with similar instruments in the central HP borehole and the surrounding satellite boreholes. Temperature distribution, strain, and brine movement will be monitored with thermocouples, fiber-optic distributed strain (DSS) and temperature (DTS) sensing, acoustic emissions (AE) monitoring, ultrasonic travel-time tomography, electrical resistivity tomography (ERT), introduced liquid and gas phase tracers, and sampling of liquid and vapor phases for natural and introduced tracers (Table 1). The test and a high-level plan for interpreting the data are summarized in Table 2, and are discussed in more detail in the following sections.

Several aspects of the test have been demonstrated and refined as part of a more informal "shakedown test" performed June 2018 through April 2019 (Boukhalfa et al., 2018), including: the dry N_2 gas circulation system, the LVDT borehole closure gage, the Drierite desiccant, the LI-COR gas analyzer, the Stanford Research Systems (SRS) gas analyzer, the packer, the grouting of thermocouples, and several revisions of the heater design. Numerical simulations by LANL and LBNL were used to refine understanding of several components of the system, supporting the design of the shakedown test and BATS. For example, the original design of the metal heater block was shown to be inefficient at transferring heat to the rock salt, and an infrared lamp heater was substituted. The new heater performed to specification and resulted in much greater heat flow into the rock salt surrounding the borehole (Stauffer et al., 2019), better achieving the goals of the test (i.e., exploring brine availability at elevated temperature). The shakedown testing has increased confidence in the BATS heater test.

In addition to providing data about brine availability, the unique brine geochemical data to be obtained are potentially relevant to long-term repository safety cases, including benchmarks for validating thermodynamic databases for geochemical modeling of brine chemistry in salt.

Table 1. Summary of boreholes (drift view illustrated in Figure 2)

Type	Purpose	Bores per array	Diameter [in]	Length [ft]	Isolation Device
HP	Heater, packer, borehole closure, N_2 circulation, gas sampling	1	4.8	12	Inflatable packer
D	Tracer source	1	2.1	15	Inflatable packer
SM	Liquid sampling	1	2.1	15	Expansion plug
F	Fiber-optic	2	1.75	18 & 30	Grouted
E	Electrical resistivity tomography (ERT) electrodes	3	1.75	18	Grouted
AE	Acoustic emissions (AE) and ultrasonic travel-time tomography sensors	3	2.1	9	Sensors on borehole wall w/ centralizer
T	Thermocouples	2	1.75	18	Grouted
SL	Cement seals with embedded strain gages	1	4.8	8	Expansion plug

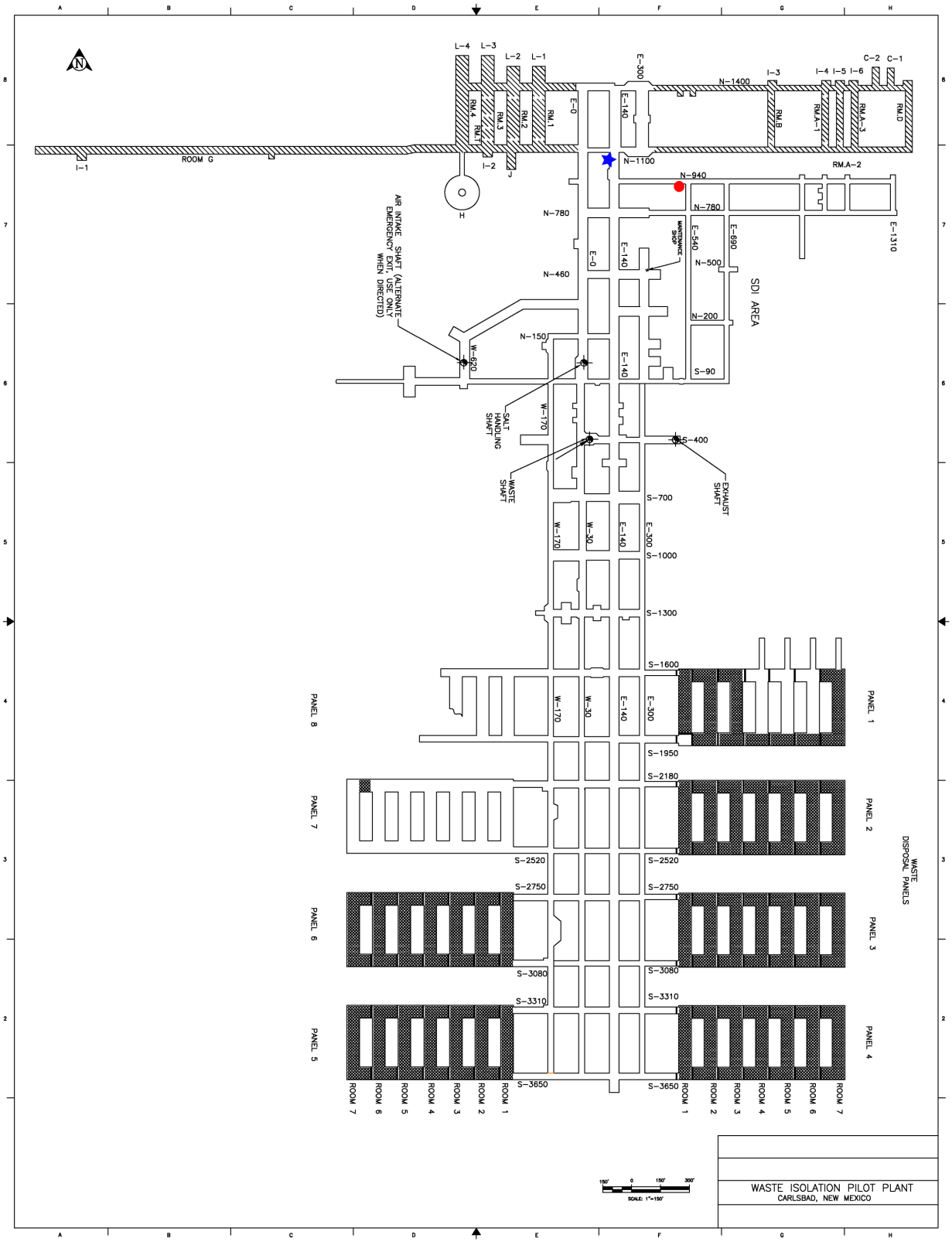

Figure 1. WIPP underground map. BATS location indicated with red circle. Shakedown test indicated with blue star.

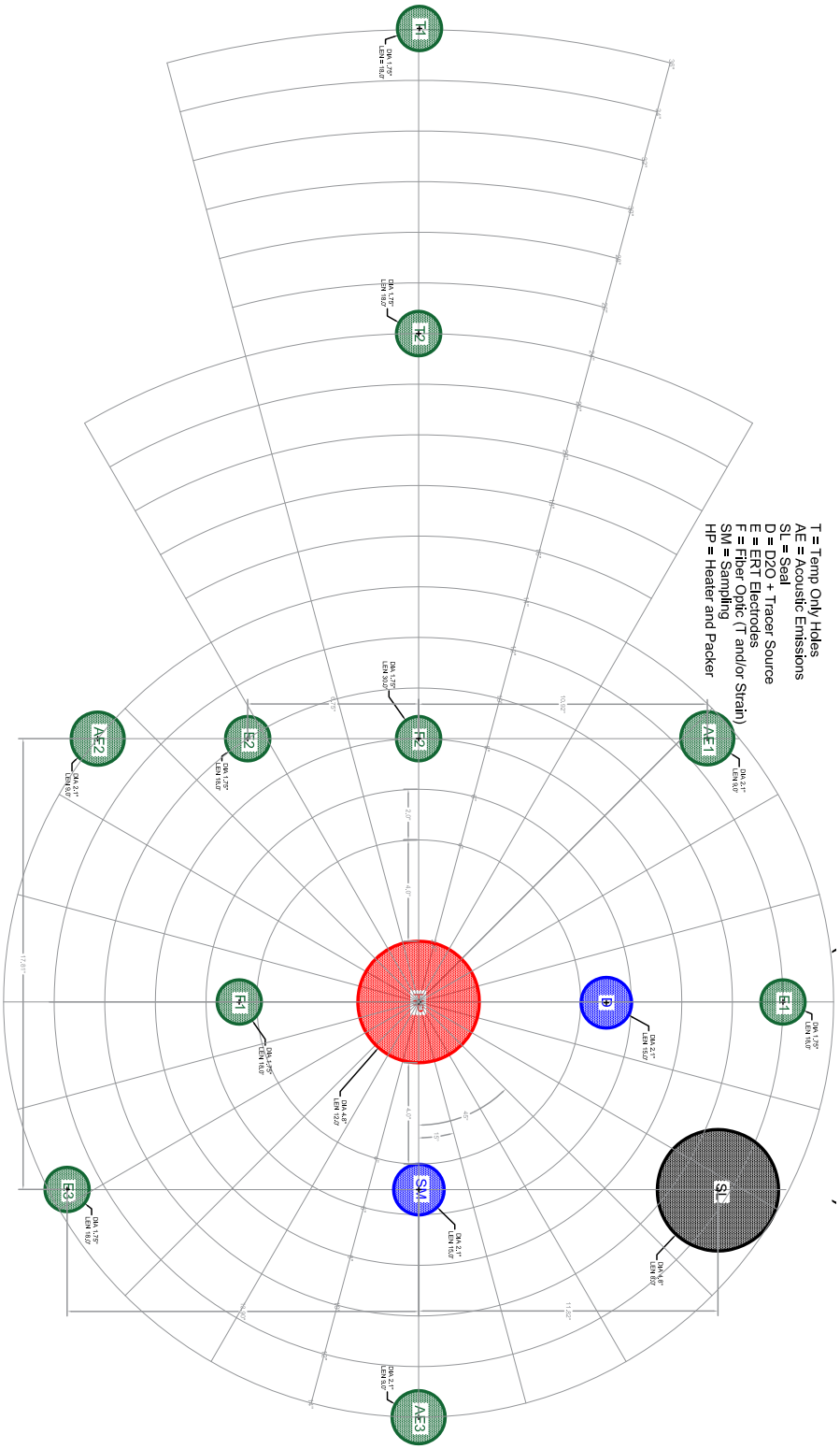

Figure 2. Borehole layout plan for each BATS test array (one heated, one unheated)

Table 2. Summary of data to be collected in BATS

Goal	Data	Location	Benefit
Quantify amount of brine in salt	Core analyses: X-ray CT, optical microscope imaging, SEM imaging, TGA analyses	Cores from HP & SL boreholes (both arrays), compared to any post-test cores	Quantify initial brine distribution in salt, including its disposition (i.e., intergranular, intragranular, hydrous minerals).
Observe changes in temporal distribution of three water types with temperature	HP: water vapor and isotopic makeup time series; SM: liquid brine samples	Continuous gas stream analysis in HP boreholes, and liquid brine samples in SM boreholes (both arrays)	Quantify initial conditions for long-term PA models (e.g., damage, pressure, saturation). Three water types differ in long-term mobility.
Estimate distribution of damage around access drift	Gas permeability testing pre- and post- heating; induced fracture characterization	HP, SL, D & SM boreholes (both arrays); borehole video surveys document significant fractures	Pre-existing damage is main source of permeability and porosity in salt
Geophysically track 4D evolution of brine during heating	ERT and ultrasonic travel-time tomograms	ERT and AE sensors (both arrays) will observe changes in brine and porosity distribution around HP boreholes	Changes in brine content and porosity due to damage and dry out are inputs to PA models and verify conceptual models
Quantify gas-phase transport through salt	Breakthrough of gas-phase tracers into HP borehole	Four gas tracers introduced to D borehole, monitored in HP borehole real-time (both arrays)	Point-to-point tracer tests provide best controls on advective gas-filled porosity and tortuosity
Quantify liquid-phase transport through salt	Breakthrough of water and liquid-phase tracers into HP and SM boreholes	Two liquid tracers, and isotopically light water introduced to D borehole, monitored in HP borehole real-time and through samples in SM borehole (both arrays)	Point-to-point tracer tests provide best controls on advective liquid-filled porosity and tortuosity
Monitor deformation and damage accumulation in salt	AE time/location distribution, borehole closure, 3D stress state, longitudinal strain along fiber	Borehole closure in HP, plug strain in SL, and longitudinal strain F2. AE triangulated from observations in AE boreholes (both arrays)	Mechanical damage and healing are main changes of permeability and porosity. AE needed to understand/predict damage that happens when heater is switched on/off
Map out 4D temperature distribution	Temperature distribution and energy input at heater	Heat source applied in HP (heated array only), temperature distribution in thermocouples (HP, T, AE, E, and F), thermistors (SL), and distributed temperature sensing fiber-optics (F) (both arrays).	Thermal properties of salt, and thermal “drive” of hydrological and mechanical systems
Observe salt/cement interactions	Microscopic, X-ray CT, and compositional analyses on post-test overcore samples of exposed cement seals	SL borehole (both arrays)	Explore stability of juxtaposed materials and understand/predict interactions between salt, brine, and cementitious materials under repository relevant conditions.

2. Testing Plan Details

The following details relate to the construction and instrumentation of BATS in general. The description of individual boreholes and their instrumentation is presented in Section 3. Tabular as-built data related to the drilling and construction are listed in the Appendix A-1.

2.1 Horizontal Borehole Drilling and Coring

The horizontal boreholes comprising each array were set to be drilled at the target diameters, locations, and orientations indicated in Figure 2 (horizontal boreholes should dip down to accumulate brine at the far ends of the boreholes). After completion of each borehole, the boreholes were blown out with compressed air to remove cuttings and a plug (i.e., a small mechanical packer) was installed to minimize long-term borehole dryout into the mine ventilation. Plugs are left in place when other activities are not being conducted in the boreholes.

The chronological progress of drilling the boreholes is illustrated in Figure 3, with the borehole names (i.e., correspondence between common names, like “unheated HP”, used here and official SDI-BH names used in WIPP documentation) and completion dates listed in Table 5. Drilling progressed through the month of February, with a pause in drilling during the month of March, related to WIPP underground scheduling and equipment availability issues. Drilling of all boreholes was completed by April 19, 2019. Both arrays are on the south side of the N-940 drift (which had an initial cross-sectional of 16.5 ft [5 m] wide by 13.5 ft [4.1 m] tall). The unheated array is further to the east (16.5 ft [5 m] east from corner of E-540 drift to center of unheated HP borehole), and the heated array is further to the west (22 ft [6.7 m] between centers of HP boreholes in two arrays). As mentioned in Figure 3 and illustrated in Figure 4, a salt “pad” was built up to raise the floor so the drilling rig could reach the elevations needed for the higher boreholes in the pattern. This salt pad remains in place and allows easier access to the boreholes. The unheated HP boreholes is located 6 ft 10 in [2.1 m] from the original floor, now covered with 2 ft [61 cm] of compacted run-of-mine salt (i.e., HP is now approximately 4 ft 10 in [1.5 m] from the top of the run-of-mine salt).

The stratigraphy of Map Units encountered in E-940 is shown in Figure 28 (unheated array would be approximately at 520 ft and heated at 500 ft x-coordinate this diagram) and Table 6. Both HP boreholes are located vertically in the Orange Marker Band (OMB), also known as Map Unit 1 (MU-1). The satellite boreholes around the central HP boreholes are spread across Map Units 0 through 3.

Figure 5 and Figure 6 illustrate the surveyed as-built state of the heated and unheated borehole arrays; Table 7 lists the as-built dimensions and coordinates of the boreholes in both arrays (i.e., the coordinates of the borehole center at the drift and back of each borehole). In the unheated array, most of the boreholes are level or dip down slightly (i.e., × connected by a dashed red line to the center of dark circle). In the heated array, several of the boreholes dip up, which required a change in the design of the brine sampling borehole (discussed later in section on SM borehole). Additionally, the unheated SM borehole was drilled at 1.75 in [4.4 cm] diameter, rather than 2.1 in [5.3 cm] diameter (as the heated SM borehole was).

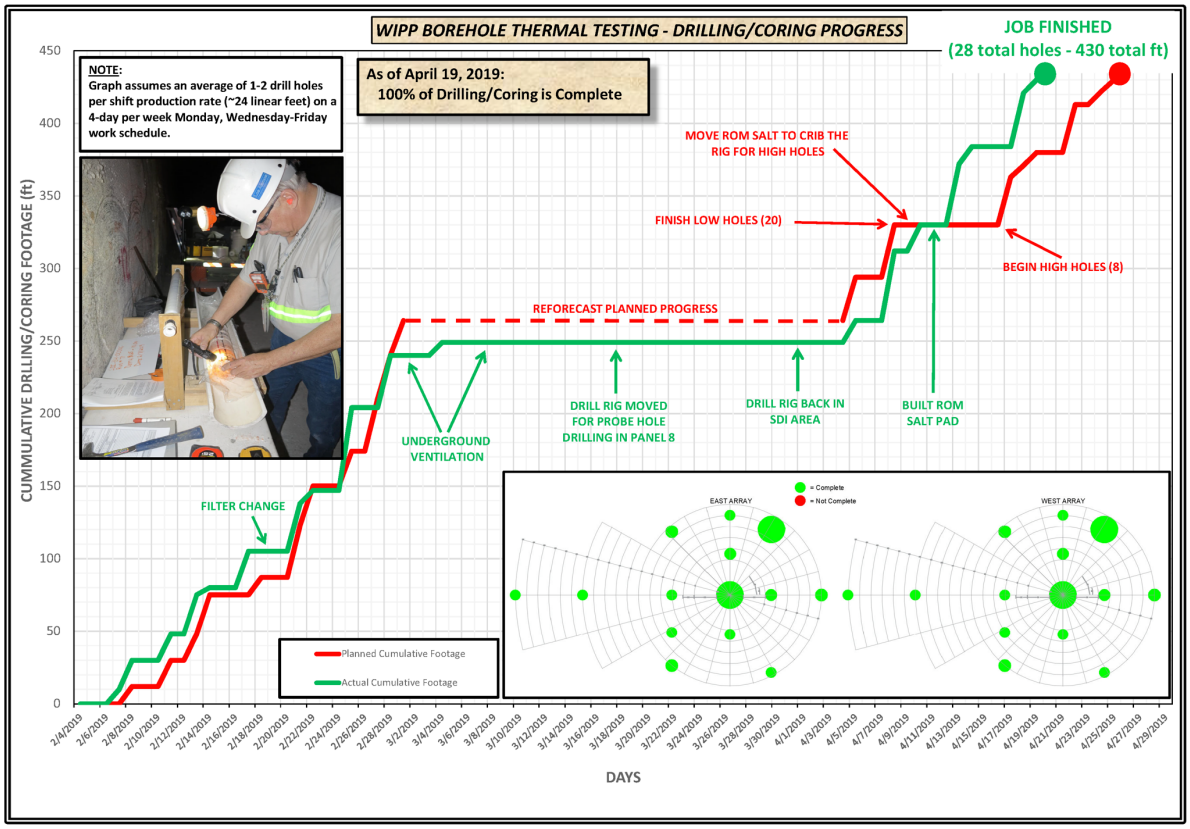

Figure 3. Final summary of progress in drilling boreholes in E-940

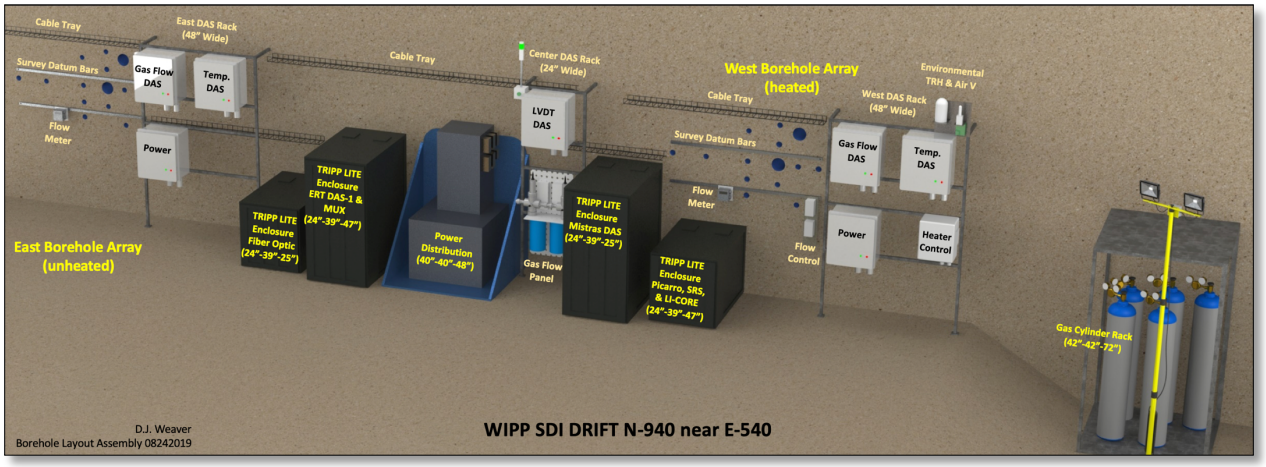

Figure 4. Layout of boreholes and instrumentation in N-940

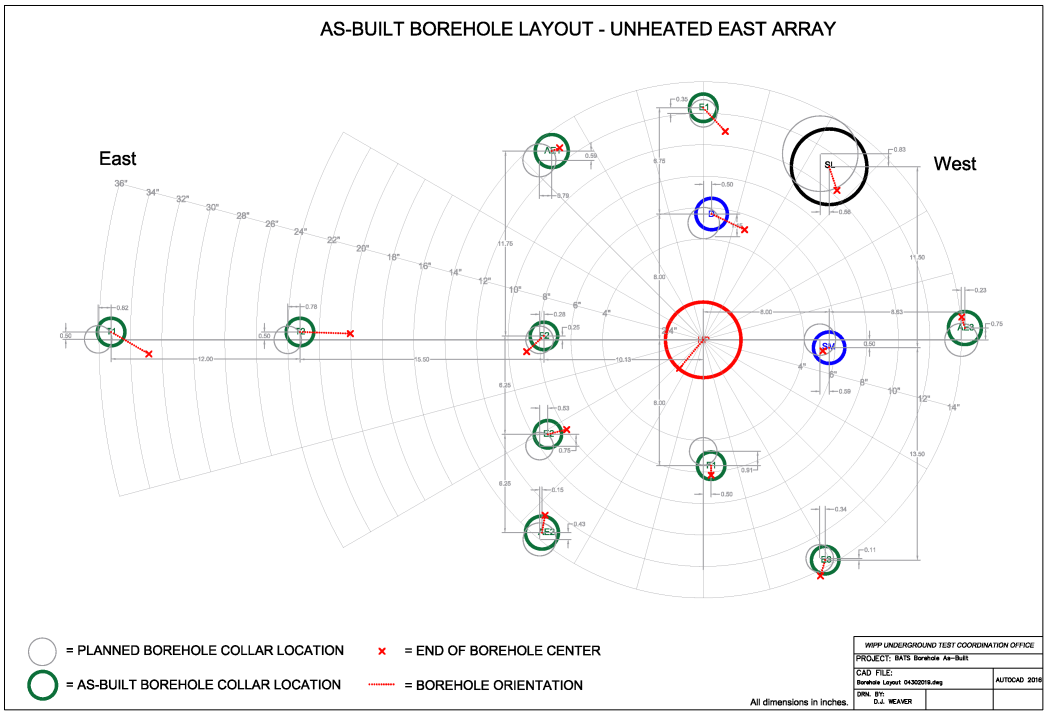

Figure 5. As-built locations and orientations of boreholes in unheated (east) array

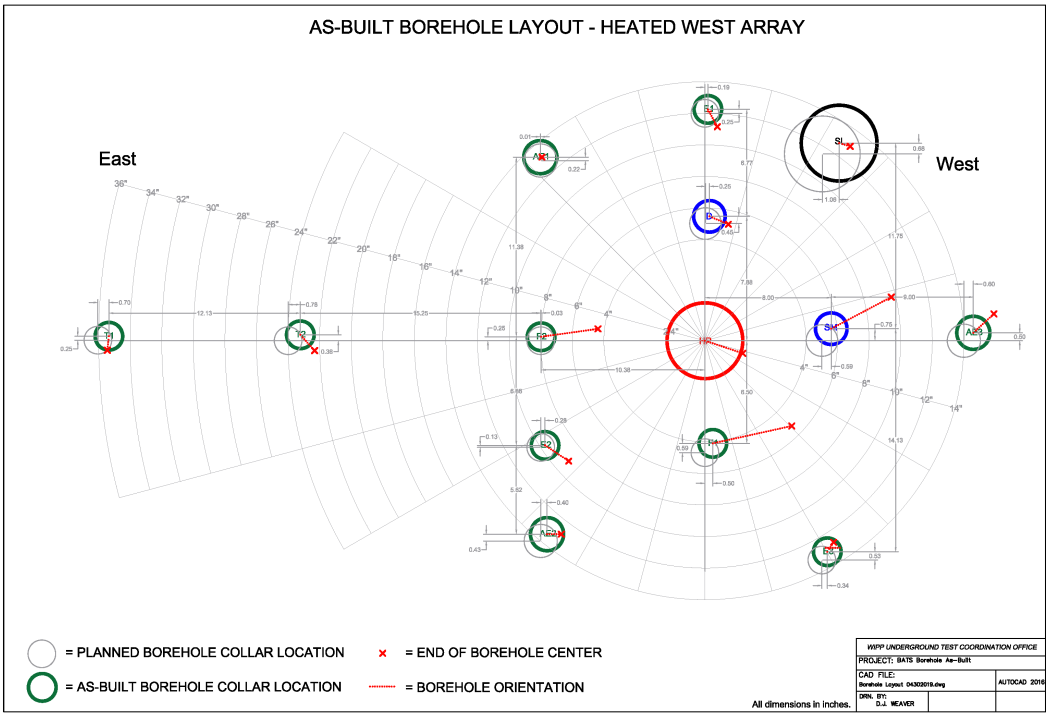

Figure 6. As-built locations and orientations of boreholes in heated (west) array

The boreholes were cleaned out with compressed air to remove cuttings and minor amounts of brine accumulated in the boreholes immediately after drilling (quantity of brine inflowing into each borehole was measured and compositional samples were collected). Brine was extracted from the rear of boreholes

using ¼-inch [0.64 cm] stainless-steel tubing connected to a vacuum pump through a sample bottle vacuum closure. This apparatus was used to collect composition samples the first time (April 18, 2019) and since then to quantify the amount of brine inflow. Figure 7 and Figure 8 show the cumulative normalized brine inflow to the heated and unheated boreholes (data are listed in Table 8 and Table 9). In these figures, brine inflow volumes were normalized by the surface area of the borehole walls. Half the boreholes (heated and unheated T1, T2, E1, E2, E3, F1 & F2) have had instrumentation grouted into them, and now can no longer be accessed for sampling.

The higher-elevation E1, D, AE1, HP, and SL boreholes (HP and the 4 boreholes above the plane of it) produced significant amounts of brine in both arrays. The T1 and T2 boreholes (furthest east of all the boreholes) also produced significant brine. The increased production of brine in the upper-elevation boreholes may be due to stratigraphic differences, with higher clay content possible in the upper layers salt.

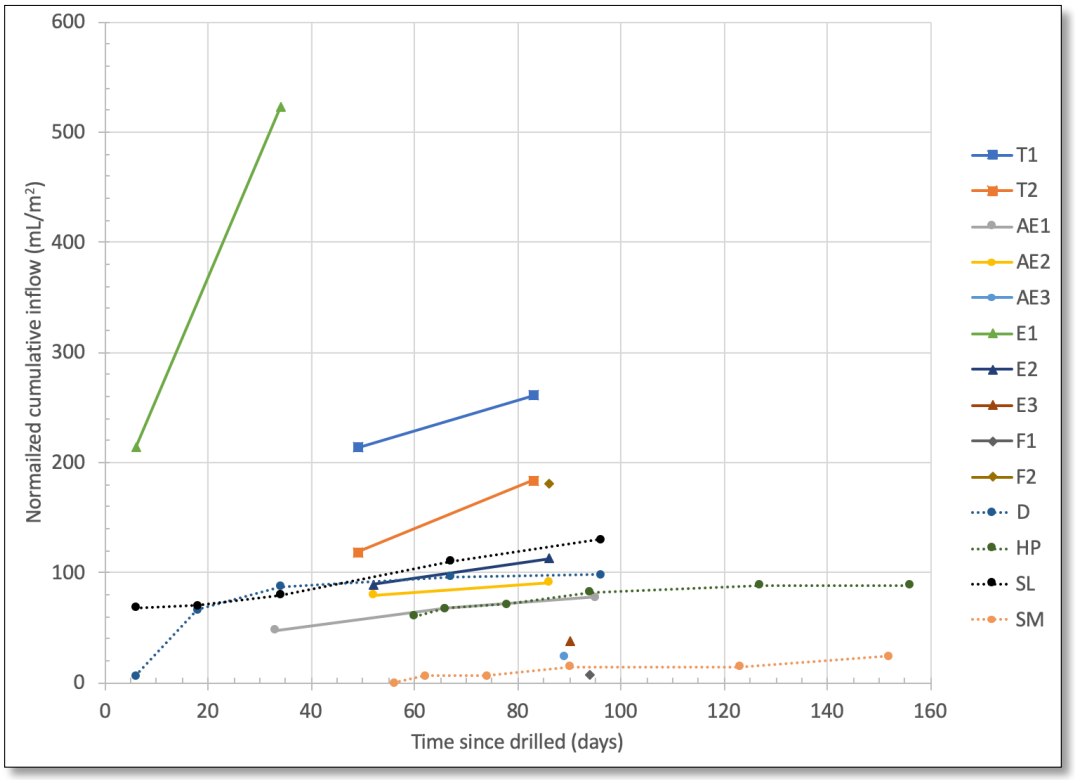

Figure 7. Cumulative normalized brine inflow from boreholes in heated (west) array

E1 produced the most brine (by far) in both arrays, which may be due to a combination of higher stratigraphic position and longer length (18 feet long). There may be a region at a certain elevation with more clay that only the longer boreholes (i.e., E1, T1, T2) can reach.

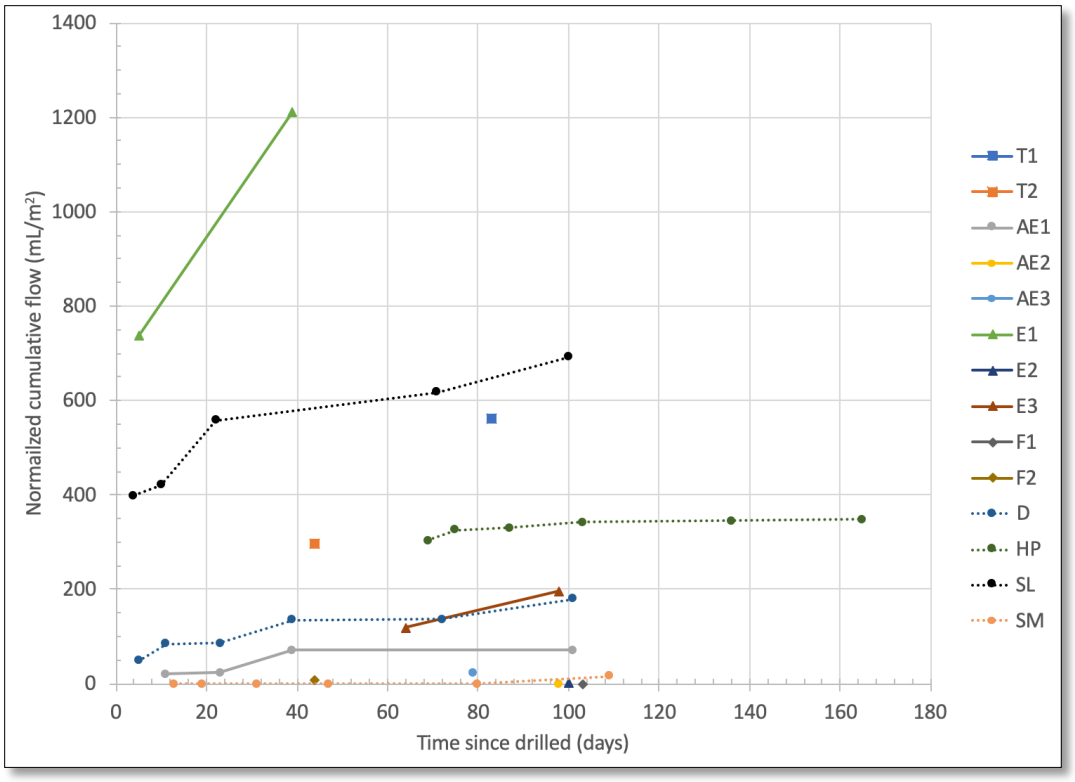

Figure 8. Cumulative normalized brine inflow from boreholes in unheated (east) array

Brine compositional samples were collected on the first sampling event. Figure 9 illustrates how the samples collected on April 18, 2019 compare to fluid inclusions and other horizons at WIPP (data listed in Table 8 and Table 9). MB-139 is about 1 m below the floor in E-940, while MB-140 is 15 m deeper into the floor below MB-139 (Powers, 2017; Beauheim & Roberts, 2002). MU-0 is below the OMB, down to MB-139 (i.e., it continues down below the where the wall intersects the floor).

The samples collected from boreholes drilled in N-940 lie along a straight line with the MB-139 samples (orange stars and circles), May 2018 E-140 sample (red square), and MU-0 samples (red empty circles), but are distinctly different from the MU-0 sample in E-140 collected in 2018 (the 2017 E-140 samples had been altered significantly by evaporation). The N-940 data, the E-140 data, Kuhlman et al. (2018) discusses more about the interpretation of these types of plots and their relation to other types of brine observed at WIPP.

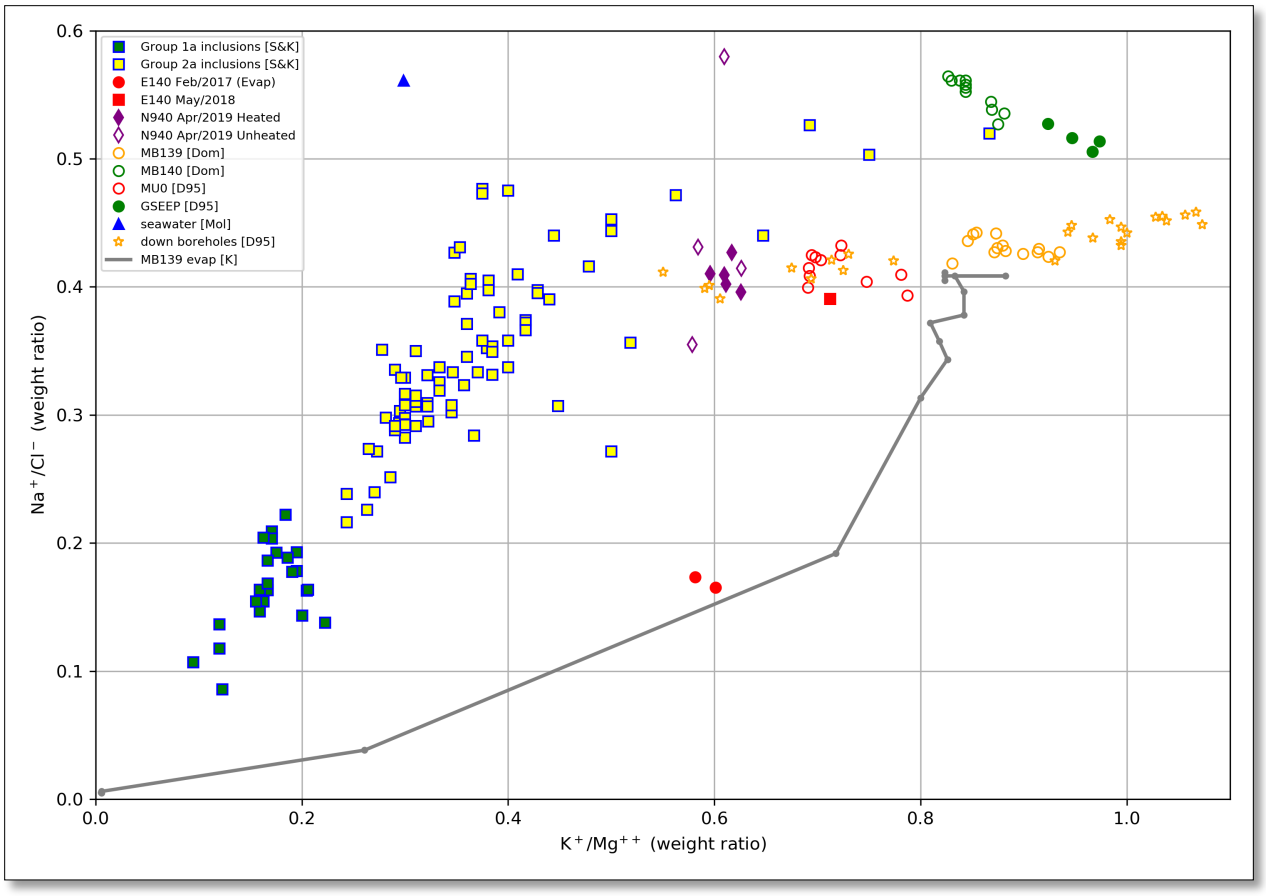

Figure 9. Mass-ratio plot of relevant Salado brines, including 2019 samples from N-940 boreholes (purple diamonds)

Table 10 lists the compositional data measured from collected samples. Cations, boron, iron were analyzed using an inductively coupled plasma optical emission spectrometer (ICP-OES), while anions were analyzed with ion chromatography (IC).

The pre-test condition of the boreholes was documented using a video inspection camera on May 6, 2019 (see example images in Figure 10). A measuring tape was used to document location of observed features, fractures, and non-salt components (e.g., regions of clay or polyhalite). On the rock face at each array, a datum bar was installed and adjusted so they are on the same plane. Because the rock face is not exactly flat, these bars provide a zero-point to measure from when installing instrumentation into the boreholes and will allow for a consistent depth of instrumentation.

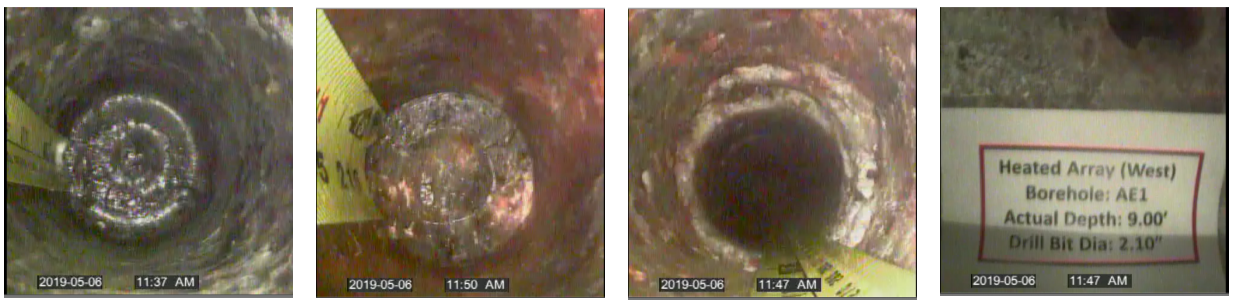

Figure 10. Example still images from borehole inspection videos

In each of the two near-identical test arrays, the central borehole is cored 12-ft [3.7 m] long, 4.8-in [12.2 cm] diameter. In the heated test, this central borehole (HP) will be heated. In both the heated and unheated tests, the HP borehole will have dry nitrogen gas circulated through it. The 4.8 in [12.2 cm] diameter seal borehole (SL) was also cored. The surrounding satellite boreholes were drilled using either 2.1-in [5.3 cm] diameter bit (sampling, AE, and source boreholes) or a 1.75-in [4.4 cm] diameter bit (instrumentation boreholes).

2.2 Horizontal Borehole Core

The core from the 4.8-in [12.2 cm] diameter boreholes was preserved in plastic bags to prevent dry out and was documented following established WIPP core logging procedures, but nuclear quality assurance (NQA) level-1 quality documentation or procedures are not required for this test. The core was crated and shipped to National Energy Technology Laboratory (NETL) for X-ray CT imaging (Figure 11), optical photography (Figure 12), surface elemental X-ray fluorescence (XRF) surface mapping, P-wave velocity and magnetic susceptibility profiling, and overall documentation.

Preliminary X-ray CT imaging results are presented in the Appendix in Figure 29 through Figure 32. Upon finalization of the core image and composition data by NETL, further analyses can be conducted with the data (e.g., the volume of larger fluid inclusions can be estimated). Core tests will help constrain the hydrological and mechanical stratigraphy encountered, including the porosity and water content of the salt.

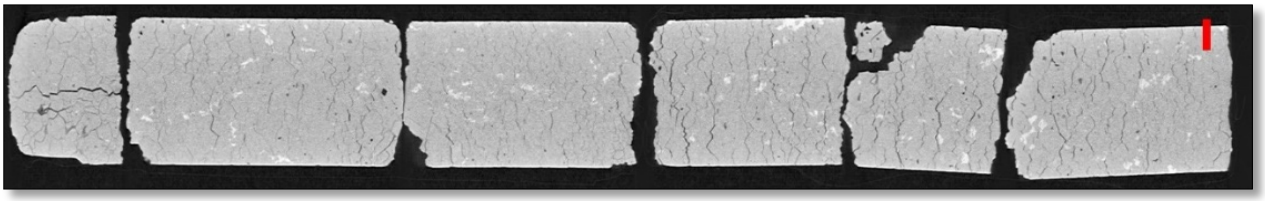

Figure 11. Example cross-sectional X-ray CT view (0-2.89 ft unheated SL) 20 mm scalebar. Fractures and fluid inclusions are darker, polyhalite is lighter

Figure 12. Example 4” diameter core (heated SL, box 1)

2.3 Gas Permeability Testing

Inflatable Aardvark-brand packers were used to perform pressure-decay gas permeability tests on the 2.1-in [5.3 cm] and 4.8-in [12.2 cm] diameter boreholes after drilling. The permeability testing packers are similar size but have fewer pass-throughs than the packers to be installed long-term into the HP boreholes for the gas circulation portion of the test. The permeability testing results will be summarized in an upcoming LANL milestone report.

2.4 Grouting of Instruments into Horizontal Boreholes

The sensors installed in the 1.75-in [4.4 cm] diameter thermocouple (T), electrical resistivity tomography (E), and fiber-optic distributed sensing boreholes (F) were grouted into place. The grout recipe (Table 3) was slightly modified by adding more water to make it less viscous and easier to pump. It was pumped down the inside of a ¾-in [1.9 cm] flush-joint polyvinyl chloride (PVC) conveyance pipe, with the sensors attached to the pipe (inside or outside the conveyance pipe). The grout flowed back towards the drift face along the outer annulus.

Table 3. Grout for instrument boreholes

Material	Amount by weight
Cement	49.5 %
Attapulgite	5 %
Run-of-mine salt	12.5 %
Water	33 %

Centralizers (additively manufactured plastic spacers) were added to the outside of the conveyance pipe to help ensure a uniform grout annulus, reducing air bubbles between the sensors and borehole wall. A collar (i.e., annular ring) was be attached to the outside of the ¾-in [1.9 cm] PVC conveyance pipe near the drift wall to prevent the grout from flowing out into the drift and to apply some back-pressure to get the grout to better fill the annulus. The ¾-in [1.9 cm] PVC conveyance and grouting pipe included ball valves left in place to prevent grout from flowing out of the tube after removing the grout pump (i.e., after grouting, but before the grout sets).

For boreholes longer than a single 10-ft [3 m] joint of PVC pipe, flush-joint PVC pipe was used to minimize grout plugging in the annulus at joints. The rough amount of grout expected to be used (i.e., based on length and diameter of the borehole) and the amount actually used were documented (Table 11). This was an additional check to confirm there were not large amounts of air (too little grout) or flow into intersecting fractures (too much grout).

2.5 Heater Test, N_2 Circulation, and Tracer Addition Sequence

Following permeability testing of the 2.1-in [5.3 cm] and 4.8-in [12.2 cm] diameter boreholes, the long-term HP borehole packers were installed; the AE sensors will be inserted into their boreholes on centralizers (not yet done at the time of this writing); the T, E, and F sensors were grouted into their boreholes; and finally the flow of dry N_2 gas will be initiated through the central (HP) borehole plumbing. The smaller-diameter 1.75-in [4.4 cm] boreholes cannot be packer tested for permeability, so instrumentation was installed in them via grouting soon after drilling was complete.

Two initial tests will be conducted at each array at the same time. As part of the first test, 1 month of background data, associated with flowing N_2 and measuring geophysical properties, will be collected before turning on the heater. One additional month of data will be collected after turning on the heaters, before adding the gas tracers to the D borehole, to observe the natural tracer response (e.g., geogenic gases and natural water vapor) of the salt to heating. We hope to observe any difference in gases produced by the salt due to heating before adding gas tracers. Gas samples will be collected from the drift air in Mylar (biaxially-oriented polyethylene tetraphthalate) bags to check for evidence of tracer gas leakage into the access drift.

The first test will be heated for ~6 months (to allow the flow system to approach a steady-state during heating), followed by a cool-down period of up to two months (to allow any thermal over-pressurization to decay away). Once the system is cooled down, liquid tracers will be added to the source (D) borehole,

before turning on the heater. The heater will be turned back on for ~6 months to observe the response of the system with the liquid tracers added.

The liquid tracers will be added to the unheated test at approximately the same time they are added to the heated test, to maximize the comparability of the observed responses in the heated and unheated tests. The gas tracers will be added in a staggered manner to allow high-frequency monitoring of each test soon after gas tracers were added (accounting for the possibility there is a rapid breakthrough of gases).

3. Configuration of Boreholes and Measurement Type

This section presents the description of individual testing boreholes and the sensors in each.

3.1 HP (Heater and Packer) Borehole

There is one central 12-ft [3.7 m] long (4.8-in [12.2 cm] diameter) HP borehole in each array (Figure 2). The 750-Watt quartz lamp heater and centralized borehole-closure gage will be mounted behind the 4.5-in [11.4 cm] diameter 2-ft [0.61 m] long Aardvark packer via a pass-through 1-in [2.5 cm] steel pipe. The packer is set approximately 5-ft [1.5 m] deep into the borehole. There will be two ¼-in [0.6 cm] stainless-steel gas lines passing through the packer: one connected to ultra-high purity (UHP – 99.999%) bottled N_2 (inflow) and the other connected to the downstream gas instrumentation (outflow).

3.1.1 Handling and Analysis of Gas Streams

The downstream gas instrumentation will be comprised of a Picarro cavity ring-down spectrometer (CRDS) and Stanford Research Systems (SRS) gas analyzer on one branch, and the LI-COR gas analyzer on the other branch. The outputs of two gas analyzer branches will be fed back through Drierite desiccant canisters. The Drierite desiccant will be weighed weekly to confirm the cumulative mass of water leaving the system. Solenoid-actuated valves upstream and downstream of the gas analyzers will allow switching of the gas streams between instruments under the control of a Campbell Scientific CR1000X datalogger. Figure 13 shows the flow of gases from the two HP boreholes through the gas analyzers and Drierite desiccant.

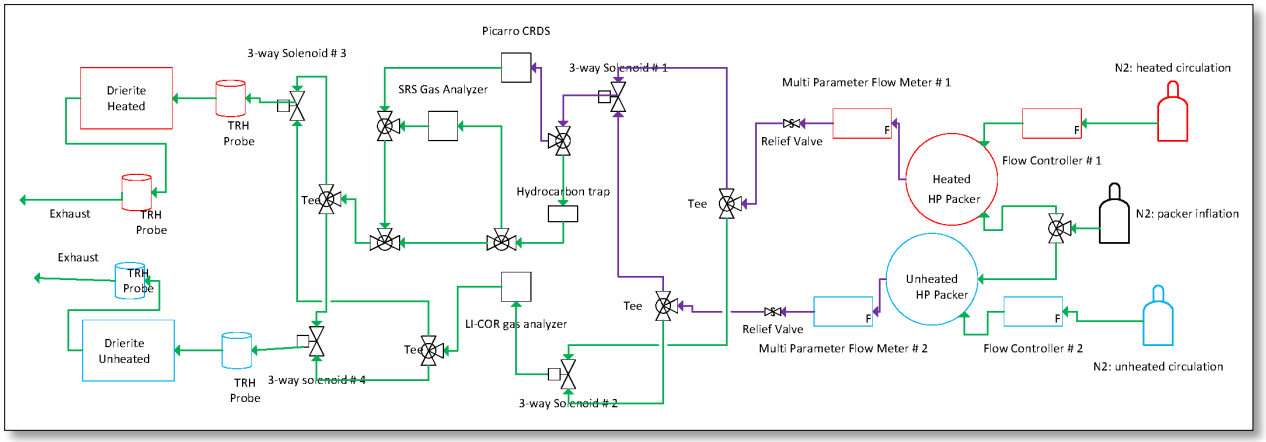

Figure 13. Plumbing of gas flow from HP boreholes through Picarro, SRS, and LI-COR analyzers. Green lines are plastic, purple lines stainless, red items are heated, blue items are unheated.

Upstream of each HP borehole, a bottle of UHP N_2 will be flowing at a constant flowrate (via a flow controller). Based on the results of the shakedown test, the test will be run at a target flowrate of 200 mL/min at standard temperature and pressure (STP). This flowrate can be adjusted up or down based on the observed brine flow into the test interval, and to test if there is a dependence of the observed water inflow rate on the gas inflow rate (previous WIPP heater test indicated there was not; Nowak & McTigue, 1987).

The mass flowrate of gas (reported at STP along with temperature and pressure for correction) will be monitored both upstream and downstream of the packer to confirm the mass balance of N_2 flowing through the system as an indication of any leaks of the packer-isolated interval through time. Downstream of the flowmeter after the packer, there will be a pressure relief valve and a pair of plumbing tees and three-way solenoid valves to allow switching the gas streams from the two boreholes between the two branches of gas analyzers instruments (Figure 13).

The Picarro CRDS, LI-COR, and SRS gas analyzers will be shared between the two borehole tests (heated and unheated). The gas plumbing will be switched between the Picarro/SRS branch and the LI-COR branch periodically via solenoid-actuated three-way valves. The Picarro analyzer reports the concentration of specific water isotopes in the gas stream (stable oxygen and hydrogen isotopes), while the LI-COR analyzer reports mmol/mol H_2O and μmol/mol CO_2. The analog outputs from the LI-COR will be connected to a Campbell Scientific CR1000X datalogger, while the Picarro and SRS gas analyzers have their own logging computers.

The SRS gas analyzer is a quadrupole mass spectrometer designed for atmospheric pressure inlet pressures. Before tracer gas is added to the D borehole, a suite of gases related to possible geogenic sources will be monitored. Just before adding the gas tracers, the SRS analyzer will be switched over to monitor a suite of gases, including the added tracers.

Before adding gas tracers (and continuing through the initial activation of the heater), we will monitor a suite of possibly enriched geogenic gases including isotopes of He [atomic mass 4], Ne [20, 21, and 22], Ar [36 and 40], Kr [84] and Xe [132] (Ballentine & Burnard, 2002). Out of these gases, ^{4}He will continue to be monitored after adding the tracer, as it is not being added to the source borehole (D), while Kr, Xe, and Ne will be added to the D borehole.

One day before adding the gas tracers to each of the D boreholes, the suite of monitored gases will be changed to observe background data. The gases to monitor after tracer addition include the primary isotope of the introduced tracer noble gases Ne [20], Kr [84], and Xe [132] will be monitored along with the primary electron fragment of SF_6 [127]. CO_2 [44] will be monitored to compare against the data provided by the LI-COR 850 instrument. Cl [35] will be monitored to assess mechanisms for production of chlorine and hydrochloric acid gas from heating the salt and brine in the borehole (Kuhlman et al., 2017). N_2 [29] (isotopologue is ~0.8% of atmospheric N_2) will be monitored to normalize the response of the instrument against variations in gas flow rate and instrument sensitivity (i.e., the gas stream will mostly be N_2). O_2 [34] (isotopologue is ~0.4% of atmospheric O_2) will be monitored to quantify the contribution of mine ventilation to the gas stream, since no processes in the borehole should generate O_2. Since only lower-concentration isotopes of N_2 and O_2 will be monitored with the other lower-concentration tracer gases, the more sensitive electron multiplier can be used without saturating the detector. At the beginning of the test (before turning on the heater), a single day of added tracer background data will also be recorded. Along with the comparison between the heated and unheated arrays, these additional background data will be used to quantify if there is a change in background between heated and unheated conditions. A hydrocarbon trap is installed after the Picarro CRDS but before the SRS gas analyzer to minimize any possible contamination from compressor oil which may contaminate the gas analyzer.

The output streams from the gas analyzers go through another pair of plumbing tees and three-way solenoid-actuated valves before passing through a pair of temperature and relative humidity (RH) probes and a canister of Drierite desiccant. The RH probes before and after the desiccant will confirm the RH of the gas stream. The final set of switching valves ensures that one set of Drierite canisters is always associated with the heated array, and one is always associated with the unheated array, even though the intervening gas analyzers are switching between arrays.

3.1.2 Heater Power

The 750-Watt quartz lamp infrared heater will be mounted on the end of the 1-in [2.5 cm] steel pipe with disc-shaped reflectors perpendicular to the 1-in [2.5 cm] pipe installed on either end of the heater to confine the radiative energy to approximately an 18-in [45.7 cm] long interval of the borehole wall. Two thermocouples will be installed, against the borehole wall (attached to the reflectors), between the borehole closure gage and the heater. The heater will be controlled by a Watlow controller set at a constant temperature of 120 to 140 °C (based on experience in the shakedown test this should be require approximately 80 to 90% of the rated power for the heater element), while a thermocouple near the borehole closure electronics will be used as an emergency over-limit check, shutting down heater power in case some malfunction leads to shorting or overheating. The Watlow controller output (applied power, current, and voltage through time) will be transmitted to a Campbell Scientific CR1000X datalogger. The hot and neutral wires for the heater will pass through the packer in a Conax fitting, while the ground wire for the power will be connected to the 1-in [2.5 cm] conveyance pipe with a brass screw clamp.

The unheated array will not have a heater, heater controller, or reflectors.

3.1.3 Borehole Closure

The borehole closure gage will be a four-arm spring steel centralizer fixed to the 1-in [2.5 cm] pipe on one end, with the other end connected to a polyetheretherketone (PEEK) slider, sliding on a notch over the 1-in [2.5 cm] pipe. The slider connects to an axial linear variable differential transformer (LVDT), which measures displacement of the slider. Displacement can be related linearly to borehole circumference. The response of the LVDT at different borehole radii will be calibrated against standard-diameter calibration rings. The LVDT is equipped with an in-line signal conditioner. The LVDT will be connected to a Campbell Scientific CR1000X datalogger.

3.1.4 Sealing Pass-through Wires

The two power supply wires for the heater (heated array only), LVDT and four thermocouples will go through the 1-in [2.5 cm] steel pipe and will be sealed at the drift face using Conax fittings. The 1-in [2.5 cm] pipe will be terminated in a stainless-steel plumbing tee. Each of the two sides of this first tee will have another tee (Two ½-in [1.3 cm] fittings on a tee on one side and two ¼-in [0.6 cm] fittings on the other tee). Each of these four tee ends will have a Conax fitting for a single type of wire (see Figure 14).

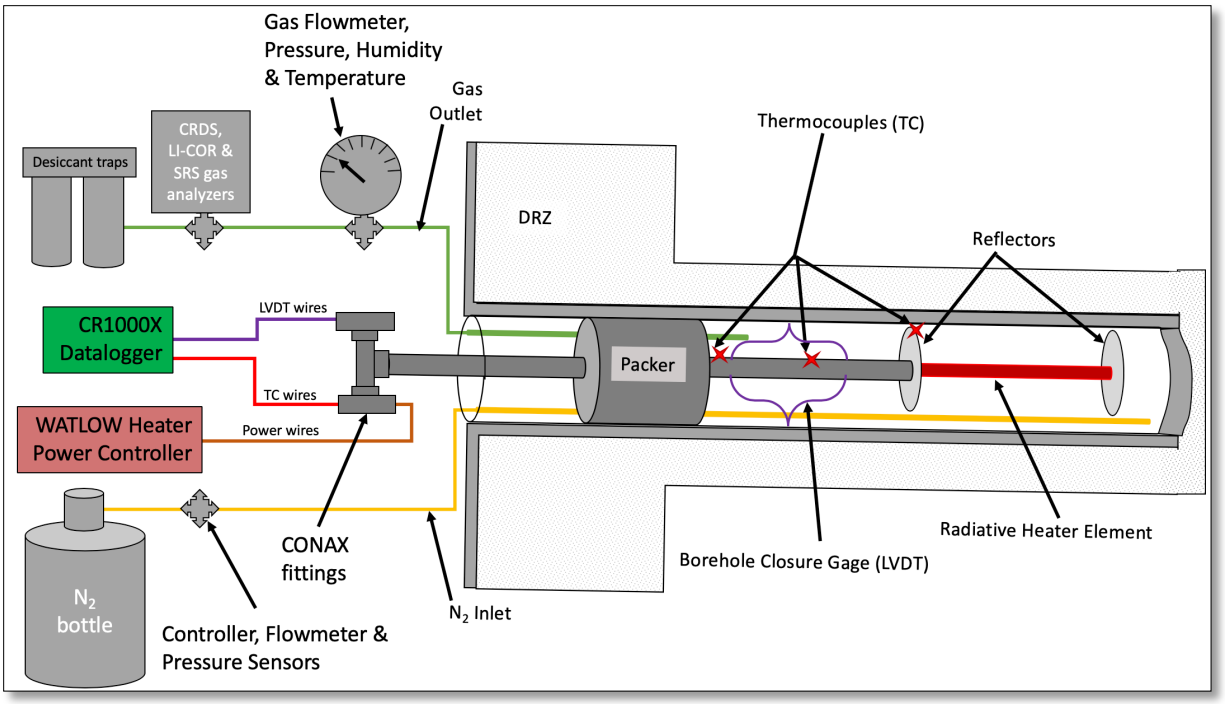

Figure 14. Wiring and plumbing diagram for the heated HP borehole

3.2 AE (Acoustic Emissions) Boreholes

There are three 9-ft [2.7 m] long (2.1-in [5.3 cm] diameter) AE boreholes (Figure 2) with initially eight piezoelectric sensors in each borehole (the 24 sensors will be moved between the heated and unheated array, but will mostly be on the heated array). The AE boreholes will not be grouted. Of the 24 sensors, 16 channels will be used to listen for AE events and triangulate the origin of individual acoustic emission events, while the other eight channels will be used as wave sources. The 16-channel Mistras data acquisition system and sensors will be used to monitor the heated borehole most of the time to capture AE generated during heat-up and cool-down. For comparison, the system will occasionally be used to monitor the unheated array, to get an estimate of the unheated background noise. There will be thermocouples in contact with the borehole wall by each centralized piezoelectric sensor (i.e., also eight per borehole). The thermocouples and piezoelectric sensors will be located on separate centralizers. The three AE boreholes are arranged in a triangle surrounding the heated borehole.

The AE sensors are installed on the arms of Quick-ZIP centralizers (made of polyoxymethylene plastic; POM) on the outside of a ¾-in [1.9 cm] stainless-steel hollow-tube conveyance. The faces of the piezoelectric transducers will be glued to half-spherical balls, which act as wave guides to ensure good contact between the transducers and the borehole wall. The piezoelectric transducers will be oriented to be on the arm of the centralizers closest to the HP borehole to optimize detection of the first arrival (i.e., P-wave) of acoustic emissions from the heated borehole and ultrasonic pings from other sensors. The Mistras system will automatically pick AE events based on a magnitude threshold, but the system also records the full stream of digitized data, which will be analyzed and post-processed elsewhere.

Multiple times during the test (e.g., at least two times before, two times during, and two times after heating) the eight piezoelectric sensors not connected to the Mistras system for AE observation will be excited with a square wave “ping,” while the other 16 sensors are listening to measure ultrasonic wave travel time between sensors (i.e., ultrasound travel-time tomography). This requires an external square wave generator since the system configuration only allows for one source channel. The ultrasound travel-time tomography test will also be conducted in the unheated array for comparison against the heated

array. If at any time the AE boreholes do not have sensors in them, they will be plugged to prevent dry out.

The piezoelectric sensors have 9.8-ft [3 m] leads, which are attached to an in-line signal conditioner box at the drift face. The cable from the signal conditioner to the Mistras control computer does not have the same cable-length constraints. The Mistras logging system with 16 channels is a computer connected to a keyboard and mouse rack-mounted inside a NEMA enclosure.

3.3 T (Thermocouple) Boreholes

There are two 18-ft [5.5 m] long (1.75-in [4.4 cm] diameter) T boreholes (Figure 2) with 16 thermocouples in each (grouted outside ¾-in [1.9 cm] PVC conveyance pipes—see Section 2.4). One of the boreholes is at 24 in [61 cm] radial distance away from the edge of the heated borehole (T2), and the other at 36 in [91 cm] radial distance (T1). Thermocouples will also be located in other measurement boreholes to increase the density of observations and help correct other observations for local temperatures. The thermocouples will be read on Campbell Scientific CR1000X loggers.

3.4 E (Electrical Resistivity Tomography) Boreholes

There are three 18-ft [5.5 m] (1.75-in [4.4 cm] diameter) E boreholes (Figure 2) with 16 electrical resistivity tomography (ERT) electrodes (12-in [30 cm] spacing between adjacent electrodes) in each, grouted outside ¾-in [1.9 cm] PVC conveyance pipes (Section 2.4). The electrodes will be driven by Multi-Phase Technologies ERT controller (MPT DAS-1), located in a NEMA enclosure in the drift. Combining the heated and unheated arrays, there will be total of six ERT boreholes with a total of 96 electrodes. Because the DAS-1 system only has 64 electrode positions, an additional multiplexing unit (MPT-MUX) with an additional 64 electrodes will be added. The ERT controller and electrodes were tested in borehole at WIPP as part of the shakedown testing. Five thermocouples will also be grouted in place with the ERT electrodes for each borehole. Based on shakedown test experience, the thermocouples are known to read anomalously high temperatures during ERT surveys (i.e., when applying current to ERT electrodes) when located in the same boreholes as the ERT electrodes.

A complete ERT survey takes <1 hour to perform for each array. They will be conducted multiple times during the test (i.e., every-other week before, during, and after heating) to measure the temporal evolution of the apparent resistivity distribution. The unheated array will be surveyed at approximately the same times as tests are performed on the heated array, to promote comparability between tests.

Apparent resistivity is a function of the salt temperature, brine content and porosity. Metal components, the presence of salt grout, and any ground control near the test arrays will impact the apparent resistivity, but these components should be fixed through time. The analysis will primarily look at the time evolution of apparent resistivity.

The ERT system will be operated only by personnel trained in WIPP electrical safety.

3.5 F (Fiber Optic Distributed Sensing) Boreholes

There is one 18-ft [5.5 m] (1.75-in [4.4 cm] diameter) F1 borehole and a second 30-ft [9.1 m] F2 borehole (Figure 2), both with grouted fiber-optic distributed sensors. The shorter F borehole has one fiber (distributed temperature sensing [DTS]), while the longer borehole has two (DTS and distributed strain [DSS] sensing). The strain fibers are attached to the outside of ¾-in [1.9 cm] PVC conveyance pipe and grouted into the borehole (see Section 2.4), with four thermocouples also grouted in with the sensors for calibration and verification. The straight DSS fiber will measure longitudinal strain along its length. The DTS fibers will be housed in small-diameter (0.04 in [1 mm]) plastic tubes before attaching to the PVC conveyance pipe and will measure temperature along the length of the fibers. For high accuracy (0.1°C) temperature measurements, a reference temperature (i.e., a water bath) will be set up. The DTS measurements can be validated or calibrated against thermocouple observations in the same borehole.

The fibers will be connected to Luna DSS and DTS receivers (IDiSi 6102 and IDiSi 6104), located in a NEMA enclosure in the drift. The thermocouples will be read using a Campbell Scientific CR1000X datalogger.

3.6 D (Tracer Source) borehole

There is one 15-ft [4.6 m] (2.1-in [5.3 cm] diameter) D borehole (Figure 2) with an 18-in [46 cm] long 1.9-in [4.8 cm] diameter long-term packer inflated in the borehole. The tracer borehole and packer will have two different configurations for gas and liquid tracer testing. For gas tracer testing, the packer will be set at a depth of approximately 7 ft [2.1 m] into the borehole. For liquid tracer testing, the packer will be set within 2 ft [61 cm] of the back of the borehole (approximately 10.5-ft [3.2 m] depth). The borehole gas tracer test will be conducted first, then the liquid tracer test will be conducted second (Section 2.5).

3.6.1 Gas Tracers

To add the gas tracers, the 1.9 in [4.8 cm] packer will be set at approximately 7-ft [2.1 m] depth. Teflon tubing will be connected to a packer pass-through, to bring it to the drift face, and the gas tracer mixture will be added to the tubing. UHP nitrogen gas will be added until the gas pressure behind the packer is pressurized to 5 psi gage [34 kPa], then it will be shut in. The pressure of the gas tracer will be monitored while it decays, as in a pressure-decay permeability test. However, if high permeability in the gas tracer borehole (D) is found, the breakthrough of gases may be quick, and require high-frequency monitoring of each tracer addition (heated and unheated), rather than run the two tracer tests simultaneously.

The gas tracers will be a mixture of noble gases (Ne, Kr, and Xe) with SF_6, that will be added to the air behind the packer. Helium will not be added as a tracer, to better allow characterization of any natural (i.e., geogenic) release of ^4He from the salt due to heating and damage accumulation (Bauer et al., 2019). Argon will not be added as a tracer or monitored, because of its relatively high concentration in the atmosphere (~1%).

An inline SRS gas analyzer (attached to HP borehole—see Section 3.1.1) will report real-time relative concentrations of up to 10 gases with approximately parts-per-million sensitivity (including CO_2, Cl, O_2, N_2, He, Ne, Kr, Xe, SF_6). Starting just before tracer gas addition, the gas stream will also be sampled every two weeks in a Mylar bag from the central HP borehole. These bag samples will be analyzed in a laboratory with a gas chromatograph to confirm and calibrate observations of gas composition by the SRS analyzer.

3.6.2 Liquid Tracers

For the liquid tracers the 1.9-in [4.8 cm] packer will be set to create a 3-ft [91 cm] long interval behind the packer by placing the packer at approximately 10.5-ft [3.2 m] depth (Teflon tubing will be connected to the packer pass-throughs to bring them to the drift face). The liquid tracers will be added to one of the pass-throughs with a syringe pump. Up to one liter of synthetic WIPP brine with liquid-phase tracers (below) will be added to the back of each tracer borehole using the lower elevation pass-through. The brine (Table 4) will be similar to the G-weep brine (GWB) recipe (Xiong, 2008), and will be formulated from an average of samples collected from the interval in April 2019.

The upper pass-through will be left open to allow gas to escape from the interval while filling with brine. Once the interval will not take more brine without flowing out, the upper pass-through will be capped off and the head space in the packer interval will be pressurized to 5 psi gage [34 kPa] with N_2. The added gas pressure will be monitored in time (like a pressure-decay test), then the pass-through will be capped off.

Table 4. Liquid tracer recipe (g salt/L solution)

Salt	GWB (Xiong, 2008)
NaCl	179.61
KCl	34.84
LiCl	0.19
$Na_2B_4O_7 \cdot 10(H_2O)$	15.06
$CaCl_2 \cdot 2(H_2O)$	2.03
NaBr	2.74
$MgCl_2 \cdot 6(H_2O)$	207.05
Na_2SO_4	25.23

The synthetic WIPP brine liquid tracers will include:

- Water with a lighter stable-water isotopic signature than Salado brine, from a high-elevation snow source, will be used to make the synthetic brine. The stable-water isotopic signature of completed tracer will be measured, since the isotopic makeup of hydrous salts used to make the brine is uncontrolled by the manufacturer.
- An organic fluorescent tracer, Na-naphthionate (also known as 1-Naththylamine-4-sulfonic acid sodium salt hydrate), which fluoresces at 325 nm (violet/blue) will be added at a concentration of 2 mmol. This tracer has been identified as minimally sorbing in high-saline environments (Magal et al., 2008). Fluorescent tracers are detectable in the laboratory using a fluorescent spectrometer at very low levels. A "black light" flash light will be used in the field to observe the presence of the tracer during sampling and post-test coring operations. Na-naphthionate is light sensitive, so the tracer and any collected liquid brine samples for spectrometer analyses will be stored in amber bottles.
- An anionic tracer, sodium perrhenate ($NaReO_4$) will also be added at a concentration of 10 mmol. It is an anionic form of rhenium, soluble in brine and detectable at very low concentrations using a mass or optical emission spectrometer. Since it is anionic, it should act as a conservative tracer.

The prepared liquid tracer will be fully characterized for the isotopic and dissolved makeup before adding to the system. The stable-water isotope makeup of water flowing into the HP borehole will be monitored via the Picarro CRDS attached to the exiting gas stream (Section 3.1.1). The composition of the brine collected in the liquid sampling borehole will be sampled weekly and monitored for perrhenate and fluorescent dye. Liquid samples can also have their stable water isotopic makeup measured in the laboratory. After the test is complete, the salt between the source and central boreholes will be cored and sampled. Black lights will be used to characterize the distribution of Na-naphthionate in the salt during follow-up post-test coring.

3.7 SM (Liquid Sample) Borehole

A 15-ft [4.6 m] (2.1-in [5.3 cm] diameter) liquid sampling borehole (SM—see Figure 2) will be plugged beyond any large fractures near the drift wall with a sewer plug (or similar device). The plug will have a Campbell Scientific EE181-L sensor to measure air temperature and relative humidity (RH) behind it to confirm equilibrium with formation brine (~75% RH) behind the plug. This RH indicates there is not significant mine ventilation into the borehole, which would remove liquid water. The RH and temperature sensor will be logged using a Campbell Scientific CR1000X datalogger.

Through the pass-through in the plug, a ¼-in [0.6 cm] Hastelloy tube will be run to the back of the borehole. The tube will be sealed into the plug pass-through with silicone. At most times, the tube will be capped at the drift face. Because the heated SM borehole dips up (Figure 6), a 5-ft [1.5 m] long mechanical packer was installed (to get the packer beyond most of the drift DRZ), with a ring of sampling tubing at the packer element, to sample brine collecting in the borehole and flowing downhill to the packer. The unheated SM borehole was drilled at 1.75-in [4.5 cm] diameter, rather than 2.1-in [5.3 cm].

Weekly, the cap from the ¼-in [0.6 cm] Hastelloy tube will be removed to attempt to collect a liquid-phase sample from the back of the borehole. A Nalgene polypropylene fluid-transfer closure will be used to connect a portable vacuum pump to the permanent ¼-in [0.6 cm] Hastelloy tube. The closure will be connected to a larger (1 L) Nalgene sample bottle. This larger Nalgene sample bottle will be used to fill smaller sample bottles, including an amber container (with minimal head space) for fluorescent tracer analysis in the lab (black light will be used to check for fluorescence in the field). After filling the smaller sample bottles, the remainder of the brine produced from the borehole with the vacuum pump will be collected into larger Nalgene bottles. The total mass of brine collected will be estimated and recorded. The same vacuum pump can be used at both the heated and unheated arrays, but dedicated Hastelloy tubing and fluid-transfer closures will be used (one for each borehole). Fluid-transfer closures will be rinsed off between sampling events with deionized water. New sample bottles will be used for each sampling episode.

3.8 SL (Seal) Borehole

The 8-ft [2.4 m] (4.8-in [12.2 cm] diameter) SL borehole (Figure 2) will have a lab-constructed cement seal emplaced. The cement seal will have a rosette of three perpendicular Geokon vibrating wire strain gages and thermistors, and a backup VPG concrete embedment gage that only reads a single component of strain. These sensors will be installed in a cement plug in the laboratory, and that plug will be installed in the SL borehole to form a seal when the salt closes in around it. The plugs with their strain gages will be made to fit snugly (e.g., ~4.6-in [11.7 cm] diameter) into the horizontal boreholes. The seals will be pushed to the back of the seal borehole, and a sewer plug (or similar device) will be used to seal the borehole near the drift (allowing the strain gage wires through) from excessive mine ventilation. A hygrometer (Campbell Scientific EE181-L) will be installed just behind the plug to monitor the RH and temperature of the air, confirming the isolation of the interval from mine ventilation (i.e., maintenance of 75% RH). The RH and air temperature sensor wire, along with the strain gage wires, will feed through the pass-through on the plug, and be sealed with silicone.

The strain gages in the cement plugs serve two purposes. First, they will provide information regarding when the borehole creeps in around the cement plug, causing the cement plug to deform. Secondly, once the salt has made contact and loaded with the plug, the three-dimensional strain in the cement plug will provide information on the three-dimensional stress state in the rock (i.e., the stress-strain behavior of the cement plug is assumed to be well-known).

The strain gages and thermistors (three perpendicular Geokon 4242X vibrating wire strain gages—including their thermistors—and a VPG EGP-5-120 embedment gage), and hygrometer will be monitored with a Campbell Scientific CR1000X datalogger. The vibrating wire strain gages will be connected a Campbell Scientific AVW-200 vibrating wire strain gage reader through an AM16-32B Campbell Scientific multiplexer before being connected to the CR1000X. The seals will be monitored until they are cored to test the cement/salt interface after the test is complete. These seals will be left in place for an extended period of time (i.e., several months to years) after the primary heater and tracer test is complete in the HP boreholes, to allow the plugs, brine, and salt to interact.

3.9 Drift (non-borehole) Observations

Ambient drift air pressure, air temperature, ventilation (i.e., “wind”) velocity, and relative humidity will be monitored at a high frequency in the drift near the location of the boreholes. The drift weather station

will have its own datalogger. Temperature will be monitored on the drift wall, to quantify how the heat from the test interacts with the drift air. The drift thermocouple will be monitored by a Campbell Scientific CR1000X datalogger. A thermal imaging camera will also be used to document the temperature distribution on the drift wall near the heated borehole (including the location around the drift thermocouple measurement) and document any leaks or hot spots in the drift during heating.

Immediately before and after the gas tracer introduction (Section 3.6.1), grab samples of air from the drift will be collected in Mylar bags for gas compositional analysis, to discern if tracer gas is leaking into the access drifts.

4. Post-Test Samples and Analyses

Pre-test activities, as-built construction, test data collection, and sampling (during heating and cooling sequences associated with gas and liquid tracer monitoring) are described in the previous sections. This section discusses the proposed post-test sampling and analyses (after cool-down). These descriptions are preliminary as some of the analyses depend on removal of packers or other equipment from boreholes, which could be prevented by borehole creep closure.

4.1 Post-Test Gas Permeability Testing

Depending on the ability to remove the N_2 circulation packer from the HP borehole and to insert the gas-testing packers into this and other boreholes, a second round of gas permeability packer testing will be conducted in the 4.8-in [12.2 cm] (HP) and 2.1-in [5.3 cm] diameter (D and SM) boreholes. Pre-test packer permeability testing is described in Section 2.3. Post-test permeability characterization will be used to quantify the changes in apparent gas permeability and damage along the length of these three boreholes (the SL borehole will not be available, since the seal experiment will still be running).

4.2 Post-Test Over-Core

If the heater and packer can be removed safely from the HP borehole after the test, a large-diameter (~12-in [30 cm]) horizontal core will be collected across the heated region (i.e., the region between the HP, D, and SM boreholes—see Figure 15) to quantify the effects of heating and the spatially map distribution of liquid tracers in the salt. Similar core will be collected in the unheated array, for comparison of tracer movement between heated and unheated arrays. If the heater cannot be removed, smaller cores will be collected from the area between the HP, D, and SM boreholes. The SL test will also be over-cored at a later date (Section 5.13).

To reduce damage to the salt near the boreholes during the over-coring process, the boreholes could first be partially filled with epoxy, cement, or some other stabilizing sealant—epoxy was extensively used in over-coring work in bentonite by Mäder et al. (2016).

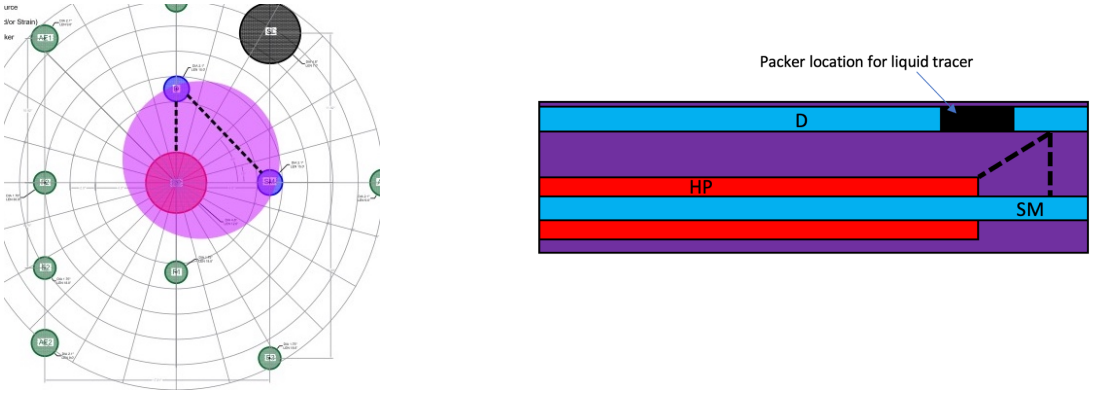

Figure 15. Post-test 12-in [30 cm] diameter over-core location (large purple circle). Drift view (left) and side view (right). Possible sub-sample transects for analyses indicated with black dashed line.

Any core collected after the test in the region where tracers were added will be checked for fluorescent tracer by ultraviolet flashlight and will be preserved in a similar manner to the way the pre-test core was collected and preserved. This core will also be sent to NETL for CT imaging and documentation. The borehole from over-coring should also be documented with borehole logging, using a black-light light source.

The ERT, DSS, DTS, and AE sensors will be disconnected before drilling the post-test core. It may be of technical value, if feasible, to continue these observations during the post-test drilling. If successful, the results could quantify the sensitivity of geophysical methods to damage or other changes induced by coring operations. The ERT survey may be difficult to conduct with drilling equipment present due to standoff distances and other electrical safety requirements. The strain, temperature, and humidity measurements in the SL borehole will continue if possible, or at least be re-connected after coring is complete.

After both pre-test and post-test cores have been analyzed via non-destructive whole-core methods, the cores will be sub-cored and sampled for laboratory microscopic (e.g., thin section petrography) and compositional analyses.

5. Plan for Data Interpretation

The components of the field test and associated data types to be collected, presented in the previous sections, are discussed in this section with regard to how the data may be interpreted. High-level summary of the data types and interpretation goals are given in Table 2. The following descriptions and interpretation plans are preliminary because the data and samples have not been collected yet. They constitute a tentative plan for additions to the technical baseline for disposal of heat-generating radioactive waste in salt. Other uses may come about after the data and samples are collected, including applications or limitations not foreseen.

In the following sections, the phrase "time series" is used to indicate a high-frequency dataset recorded automatically (e.g., thermocouple-based temperature observations recorded every few seconds), while the phrase "test results" is used to indicate a test or analysis done periodically (at least twice), but requiring manual operation or intervention (e.g., ERT, ultrasound travel-time tomography, borehole permeability testing, or liquid brine sample collection). The phrase "analysis" is used to indicate something conducted once (e.g., destructive core analyses).

5.1 Uncertainty Analysis

Uncertainty associated with the observations or instruments themselves will be estimated quantitatively and presented with the data. It is expected that such measurement uncertainty will be a minor part of the overall uncertainty associated with interpretation.

Analysis of data collected as part of the test will require fitting observations to analytical and numerical models. Two other types of uncertainty will be evaluated: 1) uncertainty associated with the structure of the models (i.e., is the correct physics included), and 2) uncertainty associated with parameter values used in the models. Different models may be used to fit the same data, and each type of model may have different complexity and epistemic model uncertainty. To the extent possible uncertainty in model results and interpretations based on them will be addressed explicitly. Modeling assumptions and other information (e.g., files and software) will be developed sufficiently to allow other researchers to replicate the results.

The BATS field test has been proposed as one of the tasks for the next round of the Development of Coupled Models and their Validation Against Experiments (DECOVALEX) international model benchmarking exercise (from 2020-2023). Sharing of data, background, interpretations, and model input files will be a natural part of this exercise. We will need to explicitly assess and discuss uncertainty to support the process.

5.2 Interpretation of Data Using Numerical Models

Given the nature of the test (i.e., geometry and coupled processes), it will likely not be possible to interpret all the data from the test using only analytical solutions, hand calculations, spreadsheets, or other simplified tools. To interpret some aspects of the test will require development of gridded numerical simulations. Results from these numerical models will then be compared to test observations, and adjustments made to improve the agreement between the models and the test data. This tuning process should achieve several goals: 1) evaluation of the conceptual models (i.e., whether the most important processes are included); 2) verification of numerical models (i.e., whether the mathematical models are being solved appropriately); and 3) better design for future field tests (i.e., what test conditions should be used, and which data collected, to validate predictive models). When possible, all aspects of the tuning process should explicitly incorporate uncertainty quantification.

In the field test, there are multiple coupled fundamental thermal, hydrologic, mechanical, and chemical processes occurring. Temperature is known to have significant effects on hydrologic, mechanical, and chemical processes. Mechanical damage influences the distribution of moisture, and chemical processes. Observed trends in seismic propagation, electrical conduction, isotope fractionation, mineral precipitation,

and RH (water activity) will be influenced by changes in temperature, mechanical state, and aqueous chemistry. Interpretation of test data will help to determine which couplings are mainly "one-way" (e.g., thermal influence on other processes) and which exhibit stronger "two-way" feedback (e.g., mechanical-hydrologic-chemical).

5.2.1 Thermal Models

Within the host salt conduction is probably the primary means of heat transfer regardless of saturation state. In open spaces (such as the HP borehole) gas-phase natural or "free" convection and radiation may also be important. Convective heat transfer may also occur where there is sufficient gas permeability and gradients of temperature (or pressure).

Heat conduction alone is probably a good approximation for heat transfer from the wall of the HP borehole to the far field. Boundary conditions, particularly at the access drift wall (i.e., perpendicular to the boreholes) may have significant influence on the observed transient thermal behavior (Stauffer et al., 2019). The source condition may be approximated numerically by a constant-temperature surface or a constant energy flux. Preliminary modeling shows the temperature distribution along the borehole wall may not be exactly constant, but more detailed cavity radiation modeling (using the Sierra Multimechanics module Aria) may be performed to develop source terms for other numerical models without radiation capabilities.

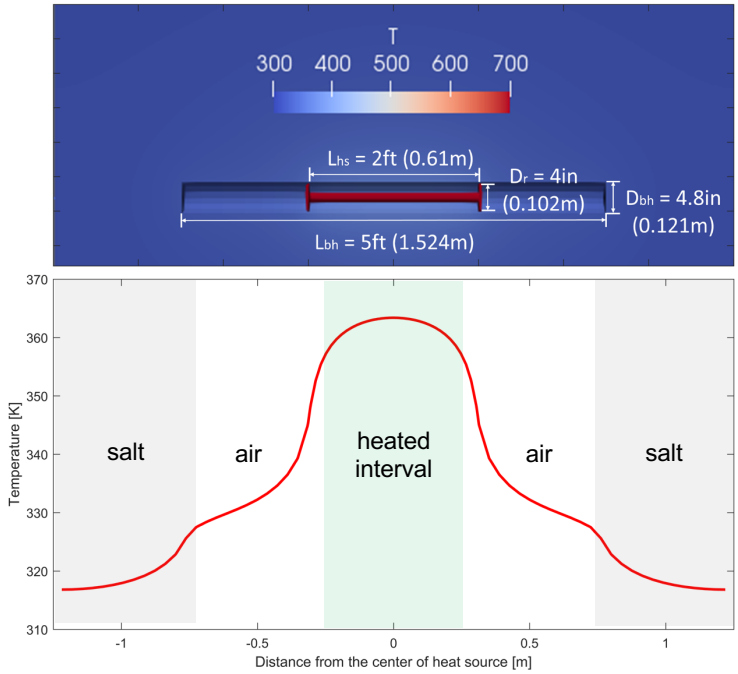

Figure 16. Preliminary cavity radiation modeling results showing borehole wall temperature due to heat source (700 K lamp) in a 4.8-in [12.1 cm] cavity with 4-in [10.2 cm] reflectors

The energy input to the salt will be determined by the power applied by the heater controller, and the model source conditions will be directly related to observations. We note that thermal conductivity for intact salt and crushed salt has been characterized as temperature-dependent (e.g., Bechthold et al., 2004).

Two-phase flow of gas and liquid through the porous medium will be incorporated to consider the boiling of brine and transport of vapor (and enthalpy) away from the heater. If liquid brine returns driven by a capillary gradient or gravity, the heat-pipe phenomenon could produce significant changes in near-field porosity (mechanical) and mineralization (chemical). Two-phase flow and storage properties of the salt

are needed to assess boiling behavior and the potential for heat-pipe activity (i.e., the capillary pressure and relative permeability as functions of saturation or water content; Johnson et al., 2019).

Temperature time series from locations throughout the salt will be used with observations of the temperature in the access drift and power input at the heater to constrain the predictions of temperature distribution in the salt.

5.2.2 Mechanical Models

The mechanical behavior of salt is elastic on short time scales, and exhibits both brittle and plastic responses (i.e., dilatory damage, and creep consolidation of openings with healing). Mechanical behavior is strongly influenced by elevated temperature (e.g., decreased stiffness, and accelerated creep strain rate). Thermal expansion or contraction of salt and brine can impact the stress state. Mechanical behavior of salt, including that around boreholes, likely has only a small impact on thermal properties and temperature distribution (i.e., one-way coupling). Mechanical behavior can be used to predict changes in hydrologic properties (i.e., volume strain can be related to permeability; Rutqvist et al., 2018).

Mechanical models can be used to predict the borehole closure observed in the HP and SL boreholes. Observations in the HP borehole will provide borehole closure information (changes in circumference) during the entire test, while the SL borehole will have three-component strain sensors embedded in cement plugs that deform once salt creep has made contact. The F2 borehole will have the longitudinal component of strain observed along the length of the 30-ft [9.1 m] DSS fiber.

Depending on constitutive behaviors, primary hydrological transport properties (i.e., porosity and permeability) of the salt could be changed by damage accumulation from heating and cooling. The distribution of damage (i.e., volume strain or changes in porosity) will be investigated using ERT and ultrasound travel-time tomography results (which jointly could discern dilatancy from dry out effects).

5.2.3 Hydrologic Models

Transport of gas and liquid brine through the salt may be strongly coupled to the temperature distribution. Thermal expansion increases the liquid pressure and can drive brine flow, with mechanically significant pressurization if the liquid permeability is low enough. The ultimate expression of hydro-mechanical coupling may be salt decrepitation, observed in the laboratory at temperatures above 250°C. Two-phase flow and transport properties of the salt (porosity, permeability, tortuosity, and capillary pressure) can all change due to both mechanical deformation and chemical dissolution/precipitation (e.g., heat pipe behavior).

Two-phase flow models will consider the atmospheric pressure boundary condition applied at the drift wall, and the high brine pressure in the far-field. The initial pore pressure distribution in the salt can be simulated by starting with an undisturbed state at the time of tunnel excavation, to estimate the distribution of pore pressure around the test (Stauffer et al., 2019). Permeability and porosity are likely highest where damage has accumulated (the access drift DRZ and to a lesser extent, damage associated with drilling boreholes). Brine saturation is probably greatest in the far field, and least where mechanical damage has accumulated.

Hydrologic models will be calibrated against water inflow time series. The distribution of dry out around the heated borehole may be inferred from ERT and ultrasound travel-time tomography.

5.2.4 Chemical Models

Aqueous chemical processes in the salt include dissolution/precipitation, which can influence hydrologic and mechanical properties, especially in connected voids (fractures, bedding planes) where transport occurs in salt. Dissolution/precipitation reactions may also influence the mineral composition of precipitates such as those in the HP borehole, and the isotopic composition of sampled water in liquid or vapor form.

Modeling of mineral phases that precipitate in the borehole uses an activity model suitable for brine (e.g., Pitzer) and it is important that the associated thermodynamic database includes data for relevant aqueous species. Kuhlman et al. (2018) showed some model predictions of the evolution of mineral phases and brine composition during evaporation or boiling of WIPP-relevant brines and laboratory evaporation experiment data. Each major source of water in WIPP salt (i.e., intergranular, intragranular, and hydrous minerals) may be distinguishable by composition alone. The data from the field test will be used to help constrain these models and assess their usefulness in quantifying brine availability.

5.3 Pre-test Brine Analysis

Brine that may have collected in the boreholes since they were drilled, before they are instrumented, has been and will continue to be collected. The boreholes were cleaned out and video logged to document their condition before installing instrumentation. The volume of brine removed from boreholes was documented and samples of it were collected for compositional analysis in the laboratory. These data provide early-time brine inflow volumes, which will be useful for calibrating hydrologic flow models, and if all boreholes produce brine, the compositional samples will provide some measure of spatial variability in the brine composition encountered in the salt. Samples will be analyzed for stable water isotopes and dissolved species components.

5.4 Core Analyses

Cores provide the best representation of rock characteristics, including m-scale to cm-scale heterogeneity encountered in the field test. They will be analyzed to describe the evaporite mineralogy and sedimentary structures. Fractures, rock damage, and core loss will be documented as well.

5.4.1 Whole-Core Analyses

The pretest 4.8 in core (HP and SL boreholes) was X-ray CT imaged at NETL. This analysis will quantify the percentage of non-halite minerals in the salt, based on the differences in X-ray absorption of different minerals. Bulk water content of WIPP salt from MU-0 is well-correlated with clay content (Figure 17). This information should provide a non-destructive estimate of bulk water content available in the salt. NETL also conducted XRF mapping on the surface of the cores, and with P-wave and magnetic susceptibility profiling. These data will help identify key mineral phases encountered in the HP and SL boreholes. Geologic descriptions of any sedimentary structures, clay seams, or induced fractures will be made.

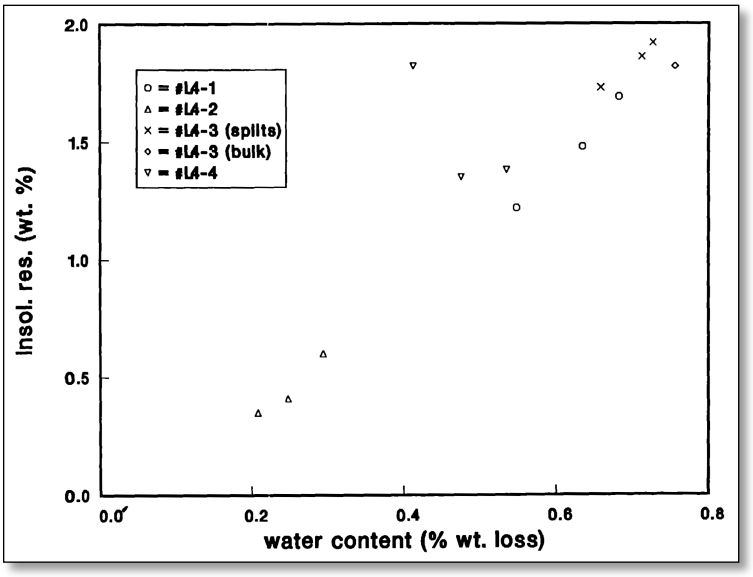

Figure 17. Bulk water content and insoluble residue (mostly clay) at WIPP salt (Finley et al., 1992)

5.4.2 Sub-Core Analyses

Small samples will be collected along defined transects (see possible transects in Figure 15) and from post-test core, to quantify the distribution of tracers (i.e., perrhenate, Na-naphthionate, and possibly water stable isotopes). These small samples will be dissolved into deionized water and analyzed by inductively coupled plasma mass spectrometry (ICP-MS) for perrhenate, and by optical fluorometry for Na-naphthionate. The distribution of tracers in the salt at the end of the test will be used to constrain models for brine flow and chemical transport during the heater test experiment, along with the tracer time series (i.e., breakthrough data for water isotopes and tracers in the HP and SM boreholes).

Several 1-in [2.5 cm] sub-cores of the salt from pre- and post-test cores subject to different amounts of damage (e.g., near drift and deeper into boreholes) will be analyzed via mercury intrusion porosimetry to estimate the connected intergranular porosity (i.e., porosity available to flow under a pressure gradient, and a measure of damage from mining and drilling) and two-phase flow properties of the salt. Porosity and capillary pressure data from near the access drift, near the heated boreholes, and in a more undisturbed state will help constrain numerical porous media two-phase flow models of the tracer test.

Representative subsamples of core (chosen to sample different mineral phases encountered, based on results of CT scan) will be destructively dehydrated for water content via thermogravimetric analysis (TGA). This will be done to identify the total water content of the salt and identify distribution of water between the three types. The evolved water during TGA may also be analyzed for stable-water isotope composition, to provide information for interpreting the CRDS data collected during the field test.

Petrographic observations using optical (e.g., reflected, refracted, and plane-polarized light) and scanning electron microscopy (SEM) of salt thin sections will be conducted on “adjacent” pre- and post-test samples (i.e., outer edge of core in pre-test sample and near the edge of borehole in post-test sample) to investigate potential impacts from heating, creep closure, and brine migration, on salt pore structure, damage-induced microstructure, and distribution of intragranular brine (i.e., fluid inclusions). Microscopic analyses may also be conducted on samples along a transect extending radially away from the heater to investigate changes in salt microstructure as a function of exposure temperature. These observations may not be used directly to quantify salt properties, but they may be used to illustrate the distribution of salt damage and deformation of fluid inclusions. Estimates of fracture density and aperture from microscopic visual inspection may help constrain the porosity of the salt. High-resolution micro-X-

ray CT may also be performed on sub-core analyses for assessment of three-dimensional pore structure and mineral distribution, which may be helpful to understand flow and deformation properties.

5.5 HP – Post-Test Borehole Precipitate Analysis

After removing the packer from the HP borehole, but before over-coring it, the salt precipitate and any liquid present in the borehole will be scraped out and both solids and liquids will be sampled. A borehole camera will be used to document the condition of the borehole and the distribution of solids and liquids in it before scraping and sampling. Precipitate samples will be analyzed using X-ray diffraction (XRD) to estimate the mineral phases present and X-ray fluorescence (XRF) to determine the elemental composition of the precipitate. The mineral phase may also be analyzed by TGA to further help identify any hydrous minerals that may have formed in the borehole through their characteristic dehydration temperature. The water phase driven off during TGA may be analyzed isotopically to further constrain the fractionation models proposed to explain the stable water isotope time series collected in the HP boreholes. The isotopic makeup of hydrous salts is possibly a point of significant uncertainty in isotope fractionation models (Krause, 1983; Clynne et al. 1981).

Any liquid phases present in the borehole will be sampled and their composition will be analyzed. These solid and liquid compositional data will be used to constrain geochemical models, which predict the mineral phases that would precipitate under the observed conditions.

5.6 Gas Permeability Test Results

Pre-test and post-test gas permeability testing will primarily provide estimates of damage and secondarily provide estimates of relative gas permeability along the borehole. The tests can be interpreted using analytical solutions for simplified geometry and single-phase gas flow, or if the results deviate from simplified solutions, they may require interpretation with a more general numerical model. Single-phase flow solutions assume the wetting liquid phase is immobile, which may be valid for gas pressures below the air-entry pressure of the porous medium. Changes in relative gas permeability may be due to changes in the salt pore structure (i.e., accumulation of damage or healing) or changes in the brine content (i.e., liquid saturation). Two-phase flow solutions involve more parameters and may not uniquely predict material properties. Data from mercury injection porosimetry analysis on sub-cores may help constrain any two-phase flow solutions used to interpret gas permeability data. Either constant-pressure or pressure-decay gas permeability tests will be interpreted similar workflows (i.e., fitting observations to a combination of analytical and numerical predictions).

Given the expected permeabilities of the salt, the gas permeability testing is primarily to characterize the extent of damage (i.e., the DRZ surrounding the access drift—see Figure 18), since the permeability of undamaged salt will likely be below the detection limit of the apparatus and the approach being used (Beauheim & Roberts, 2002).

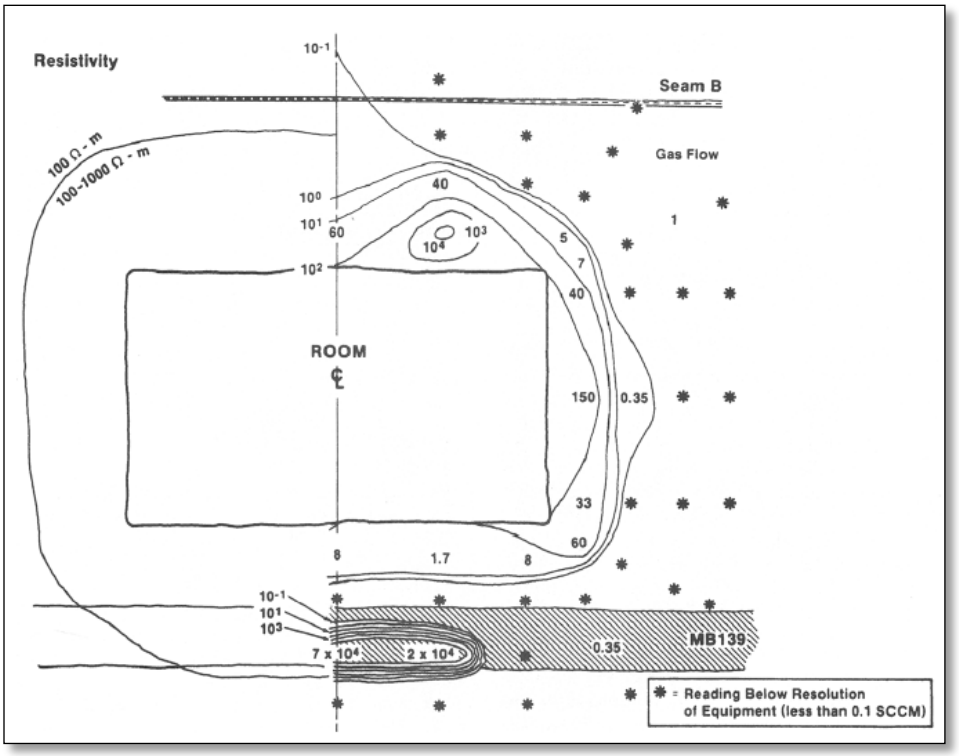

Figure 18. Results of gas flow tests and electrical geophysical surveys (Stormont 1997)

Borns & Stormont (1988) discussed the results of constant-pressure tests used to estimate the extent of the DRZ surrounding the E-1100 drift at WIPP. Blankenship & Stickney (1983) discussed procedures and results from using both falling-pressure and constant-pressure permeability tests to assess the permeability of salt in vertical boreholes surrounding a heater test at the Avery Island mine.

5.7 Data from Heater/Packer (HP) Boreholes

A large amount of data are being collected in both the heated and unheated arrays at the HP borehole. This section describes how the data streams will be analyzed.

Dry nitrogen will be circulated through the interval behind the packer. The volumetric flowrate of gas through the packed interval will be controlled and known through time.

5.7.1 HP – Water Mass Flowrate Time Series

The mass flowrate of water recovered from the packed interval will be determined at a high frequency using the downstream gas flowrate and the concentration of water in the gas. The concentration of water will be measured by either the Picarro CRDS or the LI-COR 850, depending on how the three-way solenoidal switching valve is set. The Drierite desiccant canisters downstream of the gas analyzers will be weighed approximately weekly as a check on the calculation of the total mass of water leaving the borehole system from the high-frequency flowrate data.

The Picarro CRDS will be primarily connected to the outflow of the heated array, with less-frequent data obtained from the unheated array for comparison. The LI-COR 850 gas analyzer will be connected to whichever array the Picarro is not measuring. The high-frequency water concentration time series for either array will be constructed by piecing together data from the two instruments. The plumbing is set up to have separate Drierite desiccant canisters connected to the hot and ambient arrays (i.e., these data will be lower frequency, but will not require stitching together).

The water production time series will be used to quantify the mass of water entering the borehole under heated and unheated conditions. These data will be used to estimate the relative brine permeability distribution and far-field brine static formation pressure in a porous medium flow simulation (Beauheim et al. 1997).

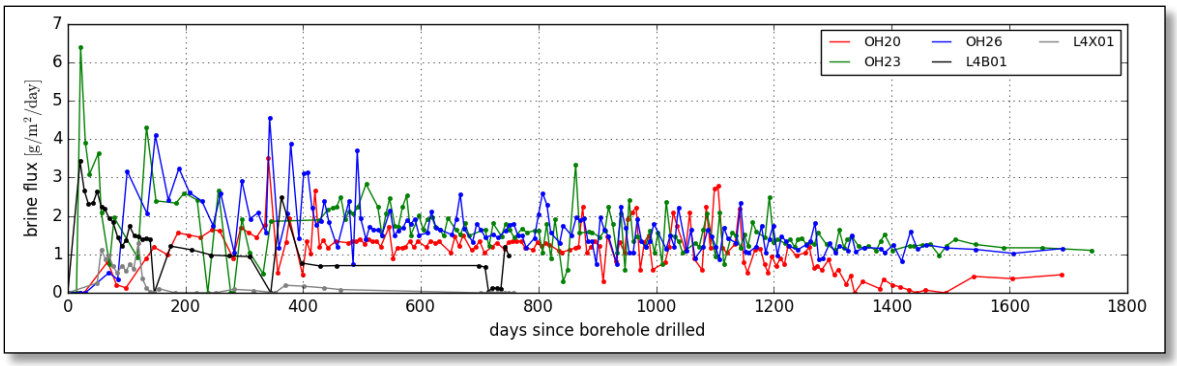

Figure 19. Brine produced from unheated horizontal boreholes at WIPP (Kuhlman et al., 2017; Data from Finley et al., 1992 and Deal et al. 1995)

Water production should be greatest just after the boreholes are drilled and will decline exponentially with time (Figure 20). The rate of water production is expected to be greater for the heated array than the unheated array (Nowak & McTigue, 1987). These data will be used to constrain numerical model predictions of both liquid and vapor water migration in the salt.

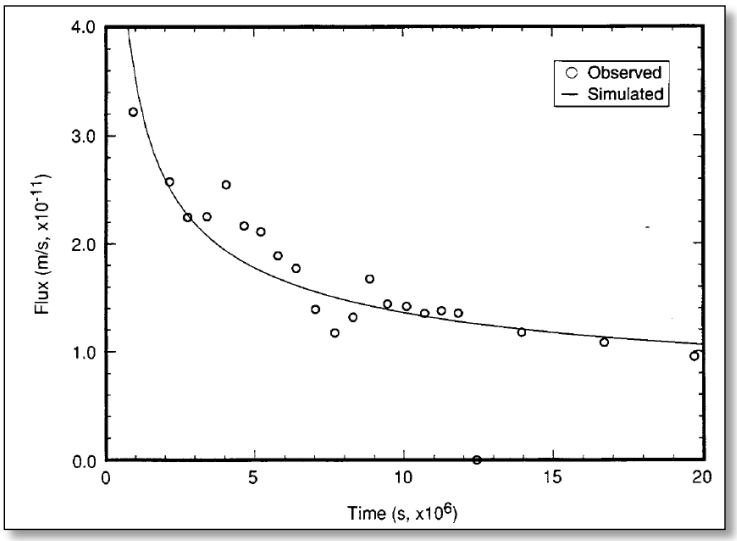

Figure 20. Comparison of McTigue (1985; 1993) model to brine inflow data from horizontal WIPP boreholes over 230 days (Beauheim et al., 1997).

The high-frequency water production time series will be a unique dataset that may show fluctuations in production due to changes in barometric pressure or mine ventilation (Figure 21). Observations of in-drift barometric pressure are needed at similar frequency to interpret results. Whenever a change in heater power occurs (up or down), brine production is expected to increase rapidly and decay exponentially (against the rapid change).

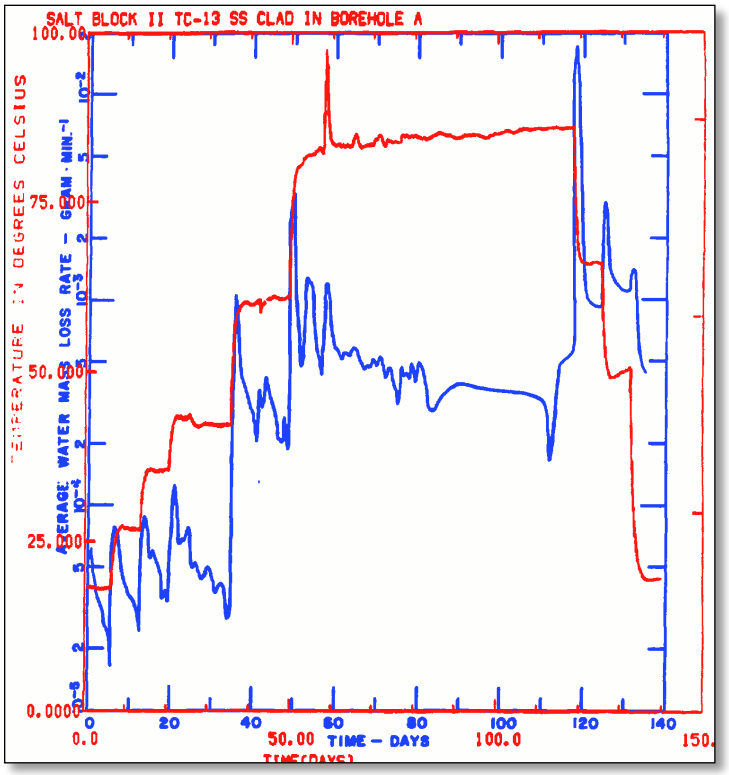

Figure 21. Water mass loss rate (blue line) and temperature (red line) observed in a large lab-scale test. Data from before 90 days were acquired by a high-frequency chilled-mirror hygrometer, while later data were obtained from daily weighing of desiccant canisters (Hohlfelder, 1979)

5.7.2 HP – Water Isotopic Composition Time Series

The Picarro CRDS will measure the relative isotopic composition of moisture in the gas stream, including both oxygen and hydrogen isotopes. The three different forms of water in the salt (intergranular, intragranular, and hydrous minerals) could have different stable-isotope signatures. The time series of water isotope fractionations may shed light on the contributions from each of the three water types before the heater is turned on, during heating, and after the heater is turned off. Isotopic differences have been observed in WIPP-relevant brine sources in the past (Figure 22). Data from WIPP fluid inclusions and anhydrite and clay layer Marker Bed 139 (MB139) show some difference in isotopic signature in historic data (Knauth & Beeunas, 1986; Lambert, 1992).

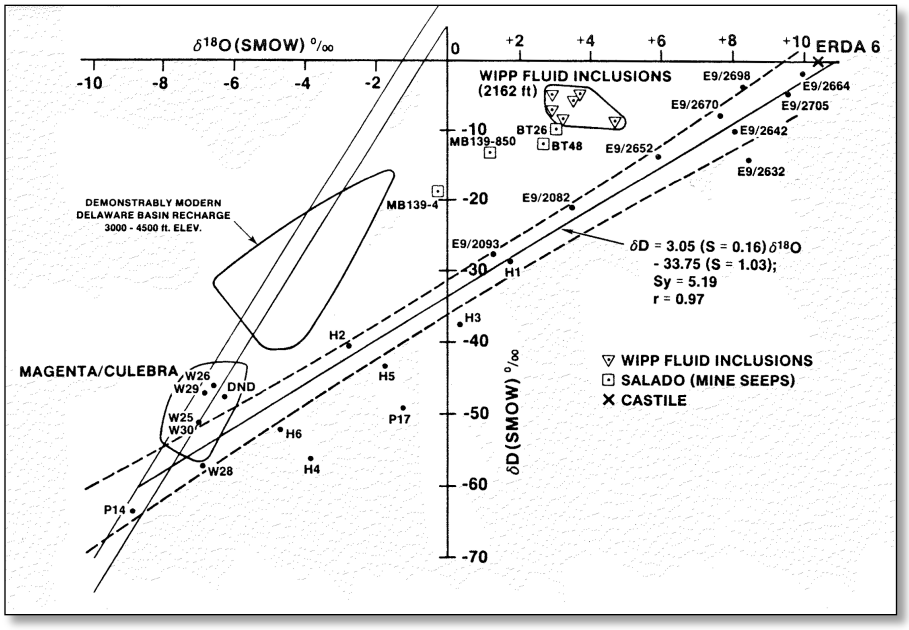

Figure 22. Stable water isotope data from WIPP site characterization studies (Lappin, 1988)

The water isotope fraction time series will be impacted by several effects: 1) evaporation as liquid brine flows into the borehole and evaporates completely or partially into the dry N_2 stream; 2) steam from dehydration of hydrous minerals, that may enter the borehole; and 3) hydrous minerals that may form in the borehole (preferentially incorporating heavier isotopes).

The relationship between δD and $\delta^{18}O$ may help detect fractionation that occurs due to evaporation in the test (e.g., Sharp, 2007; IAEA 2013). Samples will line up along evaporation lines. The difference in δD of sampled vapor could be interpretable as the fraction of tracer solution, unless brine is significantly evaporated to produce the vapor (in which case there will be a progressive shift toward heavier samples, that under-estimates the tracer fraction).

Isotopic signature time series along with brine composition from liquid samples, should help interpret how the three types of water in the salt contribute to borehole inflow under heated and unheated conditions.

5.7.3 HP – Gas Composition Time series

The gas stream from the Picarro CRDS will flow into a Stanford Research Systems Gas Analyzer (SRS QMS-200), which will record the relative concentrations of 10 different gases through time. Before the tracers are added to the D borehole, several isotopes of possible geogenic noble gases will monitored. Starting one day before introducing the tracer gases, the relevant suite of tracer gases will be modified (He, Ar, Ne, N_2, Kr, Xe, CO_2, Cl, O_2, and SF_6). These will be used to identify tracer gas introduced into the source borehole (D) and gases given off by salt (and brine) during heating, possibly including geogenic gases (e.g., isotopes of He and Ar that are trapped naturally in the salt and released due to heating or deformation).

These high-frequency data will be compared with time series of discrete gas samples collected in Mylar bags and analyzed in a laboratory with a gas chromatograph. The high frequency of data may provide a resolution of processes that cannot observed from monthly gas samples (e.g., Figure 23)

Breakthrough of tracer gases can be used to estimate the connectivity between the D and HP boreholes through the gas-filled porosity, which should be sensitive to mechanical damage and hydrologic properties (e.g., increase gas relative permeability due to dry out). The production and transport of

geogenic gases in evaporites is still an active research topic, possibly requiring further iteration on test design. If any differential breakthrough of the added tracer gases is observed, this could provide insight into chemical processes occurring in the salt. The gas tracers all have different gas-phase diffusion coefficients and solubilities in brine, each dependent on temperature. Any differential breakthrough of gases in a single test, and any difference in breakthrough of gases between the heated and unheated arrays, may help elucidate gas-liquid or gas-solid processes in the salt.

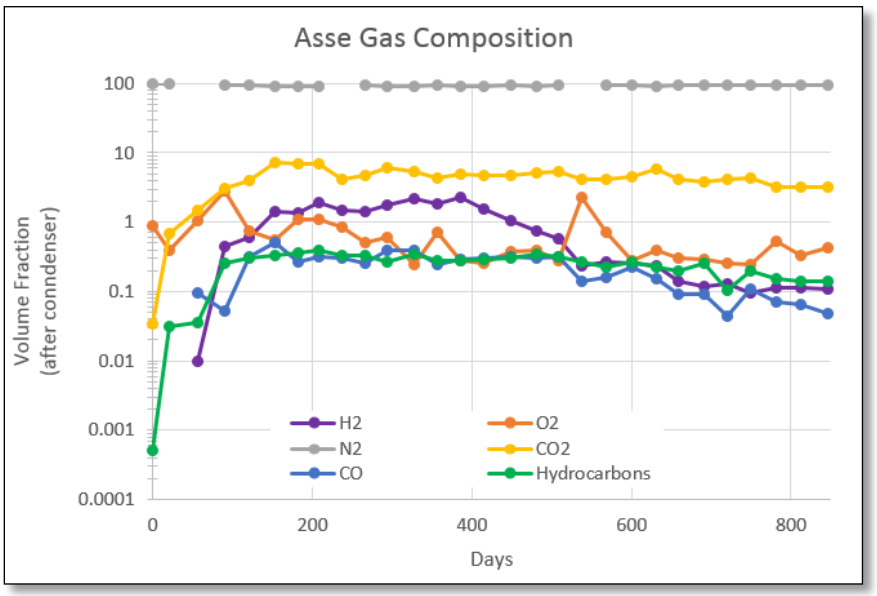

Figure 23. Non-condensable gas composition from monthly samples during Asse brine migration heater test (data from Rothfuchs et al., 1988)

5.7.4 HP – Borehole Closure Gage Time Series

The LVDT measure the closure of the HP borehole with time (i.e., change in circumference of the borehole). Borehole closure measurements can be used to calibrate numerical thermal-mechanical models of closure. The borehole closure data collected during the shakedown tests at WIPP has shown rapid, reversible changes associated with turning on and off the heater, which are likely caused directly by thermal expansion.

5.7.5 HP – Heater Power and Temperature Time Series

The heater controller will report voltage, current, and power applied to the heater, which is critical to characterizing the applied thermal boundary condition. The controller will also report the temperature at thermocouples inside the borehole used to control and provide an over-limit safety for the heater. This will be used in thermal-hydrologic-mechanical models, driving the thermal response of the entire system. Only the HP borehole in the heated array will be collecting this time series.

5.7.6 HP – Total Gas Pressure and Molar Flowrate Time series

The volumetric total flowrate of gas entering and leaving the borehole can be used to constrain the leakage of the borehole (i.e., the relative gas permeability) through time. Analysis of changes in the net leakage of the packer-borehole system through time may be used to infer temporally how any changes in permeability between pre-test and post-test results may have occurred.

5.8 Data from Acoustic Emission (AE) Boreholes

The piezoelectric transducers in the AE boreholes will be used to passively monitor for acoustic emissions and to actively conduct ultrasound travel-time tomography. Thermocouples associated with the transducers will be used to provide additional locations for monitoring the thermal response of the test to heating. A total of 16 channels which will be used between the two Mistras logging systems for the two arrays (heated and unheated). For the majority of the time the logger, as a 16-channel system, and sensors will mostly be in the AE boreholes of the heated array. At other times one or both of the Mistras systems, whether an eight- or 16-channel unit, will record data at the unheated array for comparison.

5.8.1 AE – Acoustic Emissions Time Series

The AE systems monitoring each array will be used to listen for acoustic emissions, from damage in the salt due to heating, cooling, and brine migration. The Mistras logger will automatically identify acoustic emissions, based on hits occurring on multiple channels defined by threshold crossings and similar waveform characteristics. The frequency of acoustic emissions will likely be much higher during increases and decreases in heater power (Figure 24). The AE events are associated with shear or extensional damage. This damage is associated with an increase in porosity and permeability in the salt.

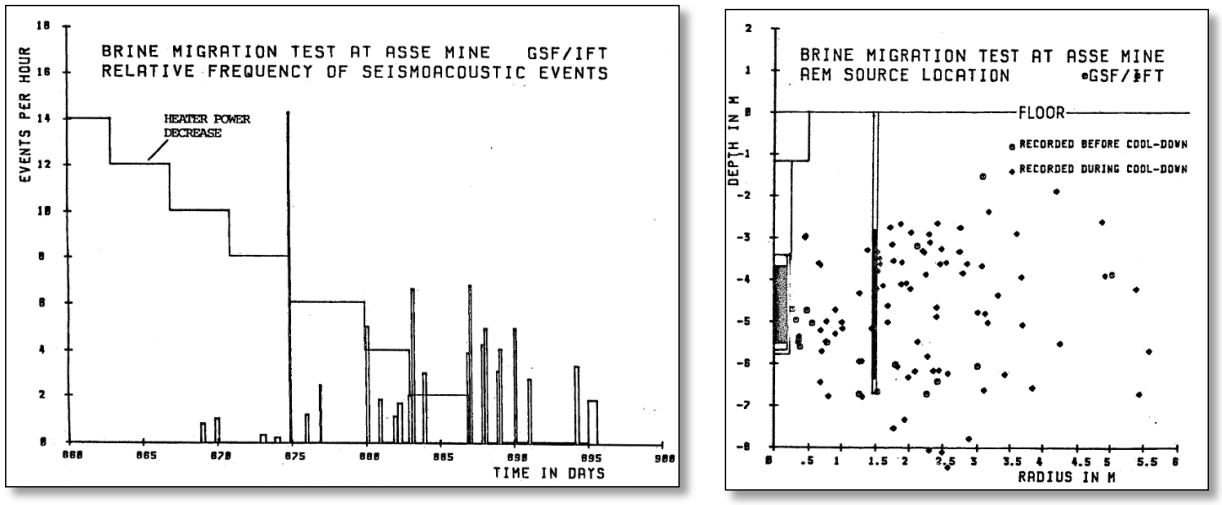

Figure 24. Acoustic emissions during Asse brine migration heater test (Rothfuchs et al., 1988)

The arrival times taken from full-waveform data digitized from the sensors can be used to locate the source of an acoustic emission (given enough of the sensors record an event to triangulate it in three-dimensional space). Estimating the source location of the acoustic emission events, provides some information on the locations of the changes in porosity and permeability.

The AE dataset can be used with the water inflow time series to validate hydrologic-mechanical flow models. The AE dataset will show where damage has occurred (Holcomb et al., 2001), which is related to where changes in permeability are occurring in the salt. Changes in porosity and permeability can impact the amount of brine flowing into the borehole and will be related to the changes in permeability between pre- and post-test gas permeability testing.

5.8.2 AE – Ultrasonic Wave Travel-Time Test Results

The eight AE sensors not used as observation locations in each array (24 piezoelectric transducers are installed in the array being listened to) can be used as sources for active ultrasound travel-time tomography. A square-wave “ping” is applied to each of the source sensors (one at a time), while listening to the 16 passive sensors attached to the Mistras system. The ultrasonic wave travel time through

the salt between each source and receiver pair is observed. This active source is driven manually, but implemented periodically (e.g., bi-weekly) to monitor any relative changes in ultrasound travel time in space and time.

The ultrasonic wave travel time through the salt is a function of compressional velocity, which is affected by temperature, porosity, heterogeneity, and brine content. The survey data will be processed by fitting a forward wave travel-time model (i.e., a straight-ray model) and incorporating changes in the resulting velocity model in terms of some or all of these effects. Changes in the velocity model can be used to refine the acoustic emissions location analysis. The ultrasonic wave travel-time tomography may be able to image changes in ultrasonic slowness around the heater. Further interpreting these changes to be due to changes in temperature or saturation may require careful laboratory testing on representative samples of salt.

Moving the sensors between the heated and unheated arrays may introduce errors or complications in the interpretation of the AE data or the ultrasonic travel-time tomography, associated with getting the sensors to the same locations.

5.9 T – Temperature Time Series

A large number of Type-K thermocouples are located in the two T boreholes, and more are co-located with other observations in other boreholes (i.e., AE, F, and E). In the heated array, the distribution of temperature observations will be used to characterize thermal conduction, and changes in the conduction with location (e.g., due to local temperature) and time during the test. Temperature data will also be used to infer the presence of convective heat transport, and to understand the thermal influence of the drift wall.

The temperature distribution will be simulated as part of thermal-mechanical and thermal-hydrologic simulations, since conduction is the primary means of heat transfer. Inside un-grouted boreholes there may be free convection. Free convection may also occur in gas-filled porosity where the temperature is greater than the brine boiling temperature (and it is likely that dewatering will occur). There will be radiation between the quartz lamp heater and the borehole wall (and re-radiation between surfaces on the wall with different temperatures). Where important, convection and radiation will be included in the interpretation of thermal processes.

Getting the temperature distribution correct is important because hydrologic and mechanical processes are driven by changes in temperatures of the salt. The mechanical and chemical properties of salt are temperature-sensitive, and brine will migrate away from regions of higher temperature because of fluid pressure associated with thermal expansion.

5.10 E – Apparent Resistivity Test Results

Electrical resistivity tomography surveys between the three ERT boreholes will be used to estimate the 3D distribution of apparent electrical resistivity in the volume enclosed by the arrays. Apparent resistivity of the salt is primarily a function of brine content and temperature, and may also be influenced by stratigraphy, differences in porosity, and man-made metal objects. The damaged region associated with an excavation tends to have higher resistivity than intact salt (Figure 18).

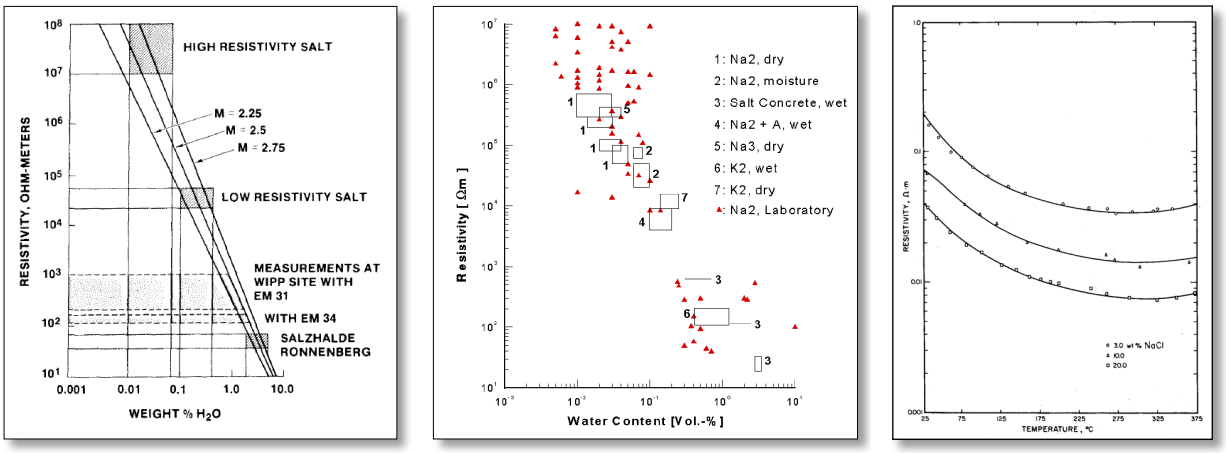

Figure 25. Left: resistivity of salt as a function of water content at WIPP (Skokan et al., 1989), (middle) and at Asse (Jockwer & Wieczorek, 2008), and (right) resistivity as a function of temperature and salinity (Ucok et al., 1980)

The interpreted ERT apparent resistivity tomograms will show changes in resistivity distribution with time. Changes in apparent resistivity can be attributed to changes in temperature and water content (Figure 25), since salt heterogeneity and added metal in the test should not change with time. ERT may be able to image an expanding dry out region surrounding the heat source, especially if the salt temperature around the heater exceeds the brine boiling point (promoting dry out). The ERT tomograms will be jointly interpreted with ultrasonic travel-time tomography and acoustic emission, to detect anomalous regions where dilation, boiling, and other processes may occur.

The ERT controller and electrodes that will be used have already been tested in boreholes at WIPP as part of the shakedown testing. The inverted results of the baseline resistivity structure and the signal from brine migration are shown in Figure 26.

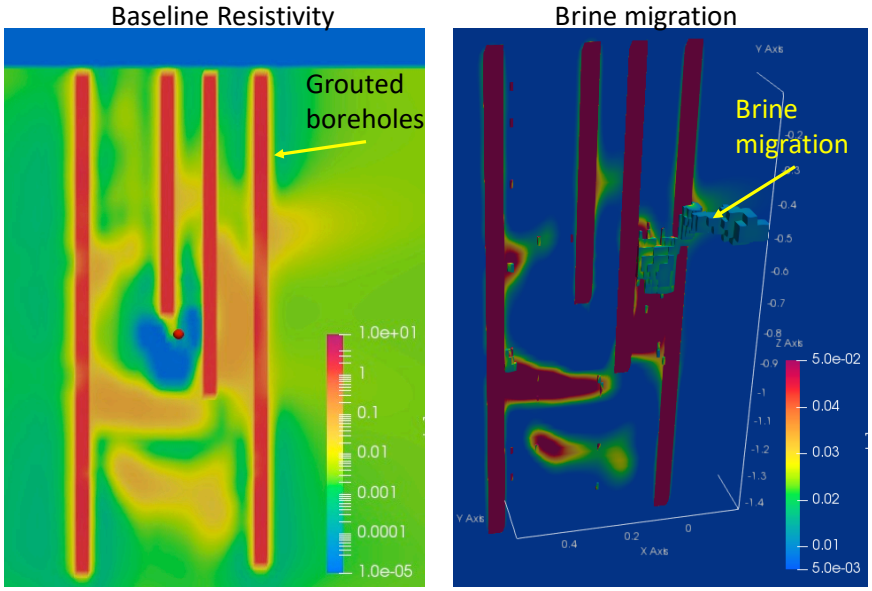

Figure 26. Baseline electrical resistivity structure [S/m] during shakedown test (left) and visualization of brine migration pathways during a brine injection test (right)

5.11 F – Fiber Optic Distributed Sensing Time Series

5.11.1 F – Distributed Strain Time Series

The longer fiber boreholes in each array (F2) will collect longitudinal strain data along the length of the fiber optic cable. The strain profile will extend into the far-field (30-ft [9.1 m] deep into the pillar) and will be used to show the deformation along the length of the F2 borehole with time. This strain measurement is precise and will be acquired at high frequency. Comparing the data between the heated and unheated arrays will quantify the timing and extent of deformation associated with heating the HP borehole. These data will be useful for validating results of thermal-mechanical simulations.

5.11.2 F – Distributed Temperature Time Series

The distributed temperature data will be a high-resolution distribution of temperature along the fiber and will complement the thermocouple data, already discussed above. Measuring the temperature distribution in the F2 borehole, will include observations more than 20 ft [6.1 m] from the heater, far away from the effects of the drift. These data will be useful in constraining and validating boundary conditions or domain size of thermal-mechanical and thermal-hydrologic numerical models.

5.12 D & SM – Source and Liquid Sample Test Results

Gas and liquid sources will be introduced into the source borehole (D). Gas-phase tracers will be monitored at high frequency in the gas stream from the HP borehole using the SRS Gas Analyzer. The stable-isotopic signature of the liquid-phase tracer will also be monitored at high frequency in the gas stream from the HP borehole using the Picarro CRDS. The liquid-phase dissolved tracers (i.e., perrhenate and Na-naphthionate) will be monitored by weekly sampling in the liquid-phase sampling borehole (SM). Liquid samples will be analyzed for changes in concentration of introduced tracers and the primary species present in the natural brine. These data will help constrain the liquid phase of flow and transport models.

5.13 SL – Seal Borehole Time Series and Test Results

The seal portion of the experiment will include strain and temperature data collection and may run for an extended period of time before the cement plugs are over-cored to observe salt/cement interactions.

5.13.1 SL – Strain and Temperature Time series

The lab-constructed seals will be instrumented with strain gages to observe strain in the salt once the borehole has closed in and made contact on the laboratory-fabricated cement plugs. The strain gages in the cement plugs will be configured to observe three components of strain and temperature (via thermistors). The strain gages in the seal will provide strain data, which is additional information to constrain a geomechanical model of borehole deformation, away from the heated borehole (assuming the properties of the cement plugs are well-known). The borehole plug at the drift side of the SL borehole will monitor RH and air temperature in the borehole between the plug and the drift.

5.13.2 SL – Salt, Brine, and Cementous Material Interactions Analysis

After the rest of the test is complete (months to years later), the SL borehole plugs will be over-cored to examine the interaction between the cements (salt concrete and sorel cement), the salt surrounding the borehole, and any brine which has flowed into the borehole during the test. Any liquid brine in the borehole will be sampled for compositional analysis before over-coring. If required for stability reasons, the open part of the SL borehole may be plugged with epoxy before over-coring (e.g., Mäder et al., 2016). The over-cored samples will be analyzed via CT scanning at NETL, just as the pre-test cores were analyzed. Sub-cores across the salt-cement interfaces will be collected for petrographic (optical and SEM analysis of thin sections), mineralogical, and micro-CT analyses. The samples will be characterized for

evidence of alteration of the salt or cementitious materials. Such investigations will include examining samples as a function of distance from the salt-cement interface.

These analyses will provide information for validation of chemical models of mineral alteration, in both the salt and cements at and in the vicinity of the salt/cement interface. As a field-scale version of experiments done as part of the Full Scale Demonstration of Plugs and Seals (DOPAS) sealing test conducted by Gesellschaft für Anlagen- und Reaktorsicherheit (GRS) (Figure 27), this test will complement the lab-scale tests that investigated the coupling between mineralogic alteration and permeability at the salt/cement interface.

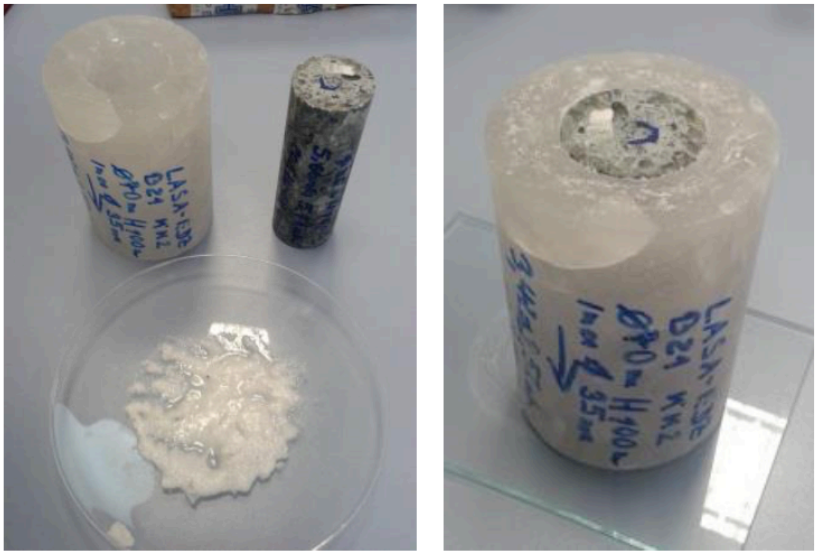

Figure 27. Laboratory-scale salt/seal interaction test at GRS (Czaikowski et al., 2016)

6. Implementation and Next Steps

During the field implementation of the BATS test at WIPP, there may be deviations from the plan laid out here. This August 2019 report is an update to the initial level-2 milestone report (April 2019) to present a nearly "as-built" description of the test, with preliminary site characterization data. At the time of this writing (August 2019), the boreholes have been drilled, the instruments have been grouted into smaller-diameter boreholes (T1, T2, E1, E2, E3, F1 and F2 in both arrays), instrumentation (i.e., Picarro CRDS, SRS gas analyzer, and LI-COR gas analyzer) has been installed and plumbed/wired into NEMA boxes, the test is nearly completely implemented. Power distribution has been recently completed by WIPP facilities and once the geophysics loggers (ERT and fiber) and AE computers are installed the testing will begin.

Lessons learned from the implementation of this field test will be considered in the design and implementation of any future field tests at WIPP. This report will be updated in FY20 with a final as-built and as-executed description of the test. Reports with the data and initial modeling interpretations will be presented as the different phases of the test continues (e.g., addition of tracers and post-test overcoring).

7. References

Ballentine, C.J. & P.G. Burnard, 2002. "Production, release and transport of noble gases in the continental crust" in *Noble Gases in Geochemistry and Cosmochemistry,* Eds. D. Porcelli, C.J. Ballentine & R. Wieler, pp. 481—538.

Bauer, S.J., W.P. Gardner & H. Lee, 2019. Noble gas release from bedded rock salt during deformation, *Geofluids* (in press).

Beauheim, R.L. & R.M. Roberts, 2002. Hydrology and hydraulic properties of a bedded evaporite formation, *Journal of Hydrology, 259*(1–4):66–68.

Beauheim, R.L., A. Ait-Chalal, G. Vouille, S.-M. Tijani, D.F. McTigue, C. Brun-Yaba, S.M. Hassanizadeh, G.M. van der Gissen, H. Holtman & P.N. Mollema, 1997. *INTRAVAL Phase 2 WIPP 1 Test Case Report: Modeling of Brine Flow Through Halite at the Waste Isolation Pilot Plant Site*. SAND97-0788. Albuquerque, NM: Sandia National Laboratories.

Bechthold, W., E. Smailos, S. Heusermann, W. Bollingerfehr, B. Barzargan Sabet, T. Rothfuchs, P. Kamlot, J. Grupa, S. Olivella & F.D. Hansen. 2004. *Backfilling and Sealing of Underground Repositories for Radioactive Waste in Salt (BAMBUS II Project)*. EUR 20621 EN. European Commission.

Blanco-Martin, L. J. Rutqvist, A. Battistelli & J. Birkholzer, 2018. Coupled processes modeling in rock salt and crushed salt including halite solubility constraints: application to disposal of heat-generating nuclear waste. *Transport in Porous Media*, 124(1):159-182.

Blankenship, D.A. & R.G. Stickney, 1983. *Nitrogen Gas Permeability Tests at Avery Island*. ONWI-190(3), Rapid City, SD: RE/SPEC, Inc.

Boukhalfa, H., P.J. Johnson, D. Ware, D.J. Weaver, S. Otto, B.L. Dozier, P.H. Stauffer, M.M. Mills, E.N. Matteo, M.B. Nemer, C.G. Herrick, K.L. Kuhlman, Y. Wu & J. Rutqvist, 2018. *Implementation of Small Diameter Borehole Thermal Experiments at WIPP*. M3SF-18LA010303014, LA-UR-29203. Los Alamos, NM: Los Alamos National Laboratory.

Borns, D.J. & J.C. Stormont, 1988. *An Interim Report on Excavation Effect Studies at the Waste Isolation Pilot Plant: The Delineation of the Disturbed Rock Zone*. SAND87-1375, Albuquerque, NM: Sandia National Laboratories.

Clynne, M.A., R.W. Potter & L.D. White, 1981. *Analytical Results of Tagged Synthetic Brine Migration Experiments at Avery Island, Louisiana*. USGS Open File Report 81-1137. Menlo Park, CA: US Geological Survey.

Czaikowski, O., J. Dittrich, U. Hertes, K. Jantschik, K. Wieczorek & B. Zehle, 2016. *Final Technical Report on ELSA Related Testing on Mechanical-Hydraulical Behaviour - LASA*. GRS-A-3851. February 29, 2016.

Deal, D.E., R.J. Abitz, D.S. Belski, J.B. Case, M.E. Crawley, C.A. Givens, P.P.J. Lipponer, D.J. Milligan, J. Myers, D.W. Powers & M.A. Valdivia, 1995. *Brine Sampling and Evaluation Program 1992-1993 Report and Summary of BSEP Data since 1982*. DOE-WIPP 94-011, Carlsbad, NM: Westinghouse Electric Corporation.

Finley, S.J., D.J. Hanson & R. Parsons, 1992. *Small-scale brine inflow experiments – data report through 6/6/91*. SAND91-1856, Albuquerque, NM: Sandia National Laboratories.

Holcomb, D.J., T. McDonald & R.D. Hardy, 2001. "Assessing the disturbed rock Zone (DRZ) at the WIPP (Waste Isolation Pilot Plant) in salt using ultrasonic waves" in *DC Rocks 2001, The 38th US Symposium on Rock Mechanics (USRMS)*. American Rock Mechanics Association. SAND2001-13055C.

IAEA (International Atomic Energy Agency), 2013. *Isotope Methods for Dating Old Groundwater*, IAEA, Vienna.

Jockwer, N. & K. Wieczorek, 2008. *ADDIGAS: Advective and Diffusive Gas Transport in Rock Salt Formations Final Report.* GRS-234, Cologne, Germany: Gesellschaft für Anlagen- und Reaktorsicherheit (GRS).

Johnson, P.J., G.A. Zyvoloski & P.H. Stauffer, 2019. Impact of a porosity-dependent retention function on simulations of porous flow. *Transport in Porous Media*, 127(1), 211-232.

Jordan, A.B., H. Boukhalfa, F.A. Caporuscio; B.A. Robinson & P.H. Stauffer, 2015. Hydrous mineral dehydration around heat-generating nuclear waste in bedded salt formations, *Environmental Science & Technology*, 5:1-13.

Knauth, L.P. & M.A. Beeunas, 1986. Isotope geochemistry of fluid inclusions in Permian halite with implications for the isotopic history of ocean water and the origin of saline formation waters. *Geochimica et Cosmochimica Acta*, 50(3), 419-433.

Krause, W.B., 1983. *Avery Island Brine Migration Tests: Installation, Operation, Data Collection, and Analysis*. ONWI-190(4). Rapid City, SD: RE/SPEC, Inc.

Kuhlman, K.L. & B. Malama, 2013. *Brine Flow in Heated Geologic Salt*. SAND2013-1944, Carlsbad, NM: Sandia National Laboratories.

Kuhlman, K.L. & S.D. Sevougian, 2013. *Establishing the Technical Basis for Disposal of Heat-Generating Waste in Salt*. SAND2013-6212P, FCRD-UFD-2013-000233. Albuquerque, NM: Sandia National Laboratories.

Kuhlman, K.L., M.M. Mills & E.N. Matteo, 2017. *Consensus on Intermediate Scale Salt Field Test Design*. SAND2017-3179R, Albuquerque, NM: Sandia National Laboratories.

Kuhlman, K.L., C.M. Lopez, M.M. Mills, J.M. Rimsza & D.C. Sassani, 2018. *Evaluation of Spent Nuclear Fuel Disposition in Salt (FY18)*. M2SF-18SN010303031, SAND2018-11355R, Albuquerque, NM: Sandia National Laboratories.

Lambert, S.J., 1992. Geochemistry of the Waste Isolation Pilot Plant (WIPP) site, southeastern New Mexico, U.S.A., *Applied Geochemistry*, 7(6):513-531.

Lappin, A.R., 1988. *Summary of Site-Characterization Studies Conducted from 1983 through 1987 at WIPP, Southeastern New Mexico*, SAND88-0157. Albuquerque, NM: Sandia National Laboratories.

Mäder, U., K. Detzner, F. Kober, H. Abplanalp, T. Baer & V. Cloet, 2016. *FEBEX-DP Plug Overcoring and Concrete-Bentonite Interface Sampling prior to Dismantling*. NAB 16-10, Switzerland: NAGRA.

Magal, E., N. Weisbrod, A. Yakirevich & Y. Yechieli, 2008. The use of fluorescent dyes as tracers in highly saline groundwater. *Journal of Hydrology*, 358(1-2), 124-133.

McTigue, D.F., 1985. *A Linear Theory for Porous Thermoelastic Materials*. SAND85-1149. Albuquerque, NM: Sandia National Laboratories.

McTigue, D.F., 1993. *Permeability and Hydraulic Diffusivity of WIPP Repository Salt Inferred from Small-Scale Brine Inflow Experiments*. SAND92-1911, Albuquerque, NM: Sandia National Laboratories.

Nowak, E.J. & D.F. McTigue, 1987. *Interim Results of Brine Transport Studies in the Waste Isolation Pilot Plant (WIPP)*. SAND87-0880. Albuquerque, NM: Sandia National Laboratories.

Powers, D.W., 2017. *Reference Stratigraphy Applied to Rock Mechanics Studies for the Waste Isolation Pilot Plant: A Review – January 11, 2017*, ERMS #567705. Carlsbad, NM: Sandia National Laboratories.

Rothfuchs, T., K. Wieczorek, H.K. Feddersen, G. Staupendahl, A.J. Coyle, H. Kalia & J. Eckert, 1988. *Brine Migration Test: Asse Salt Mine Federal Republic of Germany Final Report, GSF-Bericht 6/88*, Joint project between Office of Nuclear Waste Isolation (ONWI) and Gesellschaft für Strahlen- und Umweltforschung Munchen (GSF).

Rutqvist, J., M. Hu, Y. Wu, L. Blanco-Martín & J. Birkholzer, 2018. S*alt Coupled THMC Processes Research Activities at LBNL: FY2018 Progress*. LBNL-2001170. Berkeley, CA: Lawrence Berkeley National Laboratory.

Sandia National Laboratories (SNL), 2018. *Project Plan: Salt in situ Heater Test*, SAND2018-4673R.

Sharp, Z., 2007. *Principles of Stable Isotope Geochemistry*, Pearson.

Skokan, C.K., M.C. Pfeifer, G.V. Keller, and H.T. Andersen, 1989. *Studies of Electrical and Electromagnetic Methods for Characterizing Salt Properties at the WIPP Site*, New Mexico. SAND87-7174, Albuquerque, NM: Sandia National Laboratories.

Stauffer, P.H., A.B. Jordan, D.J. Weaver, F.A. Caporuscio, J.A. Ten Cate, H. Boukhalfa, B.A. Robinson, D.C. Sassani, K.L. Kuhlman, E.L. Hardin, S.D. Sevougian, R.J. MacKinnon, Y. Wu, T.A. Daley, B.M. Freifeld, P.J. Cook, J. Rutqvist and J.T. Birkholzer, 2015. *Test Proposal Document for Phased Field Thermal Testing in Salt*. LA-UR-15-23154, FCRD-UFD-2015-000077. Los Alamos, NM: Los Alamos National Laboratory.

Stauffer, P.H., E.J. Builtinan, S.M. Bourret & G.A. Zyvoloski, 2019. *Salt Thermal Testing in Heated Boreholes: Experiments and Simulations*. M2SF-19LA010303011, LA-UR-19-22729, Los Alamos, NM: Los Alamos National Laboratory.

Stormont, J.C., 1987. *Small-Scale Seal Performance Test Series "A" Thermal/Structural Data through the 180th Day*, SAND87-0178. Albuquerque, NM: Sandia National Laboratories.

Stormont, J.C., 1997. Conduct and interpretation of gas permeability measurements in rock salt. *International Journal of Rock Mechanics and Mining Sciences*, 34(3–4):303.e1–303.e11.

Ucok, H., I. Ershaghi, and G.R. Olhoeft, 1980. Electrical resistivity of geothermal brines. *Journal of Petroleum Technology*, 32(04), 717-727.

Xiong, Y, 2008. *WIPP Procedure SP-20-4: Preparing Synthetic Brines for Geochemical Experiments*. Carlsbad, NM: Sandia National Laboratories.

A-1. Appendix: Tabular Data

Additional data, summarized or exemplified in figures in the main text, is presented here in tabular form.

Table 5. BATS borehole completion dates and official WIPP SDI DB# names

Array	Borehole ID	SDI DB#	Date drilling complete
Unheated	F1	SDI-BH-0010	2/8/19
Unheated	HP	SDI-BH-0006	2/8/19
Unheated	E2	SDI-BH-0011	2/11/19
Unheated	AE2	SDI-BH-0012	2/13/19
Unheated	E3	SDI-BH-0013	2/13/19
Heated	F1	SDI-BH-0014	2/17/19
Heated	HP	SDI-BH-0007	2/17/19
Heated	E3	SDI-BH-0015	2/21/19
Heated	SM	SDI-BH-0016	2/21/19
Heated	AE3	SDI-BH-0017	2/22/19
Heated	AE2	SDI-BH-0018	2/25/19
Heated	E2	SDI-BH-0019	2/25/19
Heated	F2	SDI-BH-0020	2/25/19
Heated	T1	SDI-BH-0022	2/28/19
Heated	T2	SDI-BH-0021	2/28/19
Unheated	T1	SDI-BH-0027	2/28/19
Unheated	AE3	SDI-BH-0023	3/4/19
Unheated	SM	SDI-BH-0024	4/5/19
Unheated	F2	SDI-BH-0025	4/8/19
Unheated	T2	SDI-BH-0026	4/8/19
Unheated	AE1	SDI-BH-0028	4/13/19
Unheated	D	SDI-BH-0029	4/13/19
Unheated	E1	SDI-BH-0030	4/13/19
Unheated	SL	SDI-BH-0008	4/14/19
Heated	D	SDI-BH-0031	4/18/19
Heated	E1	SDI-BH-0032	4/18/19
Heated	SL	SDI-BH-0009	4/18/19
Heated	AE1	SDI-BH-0033	4/19/19

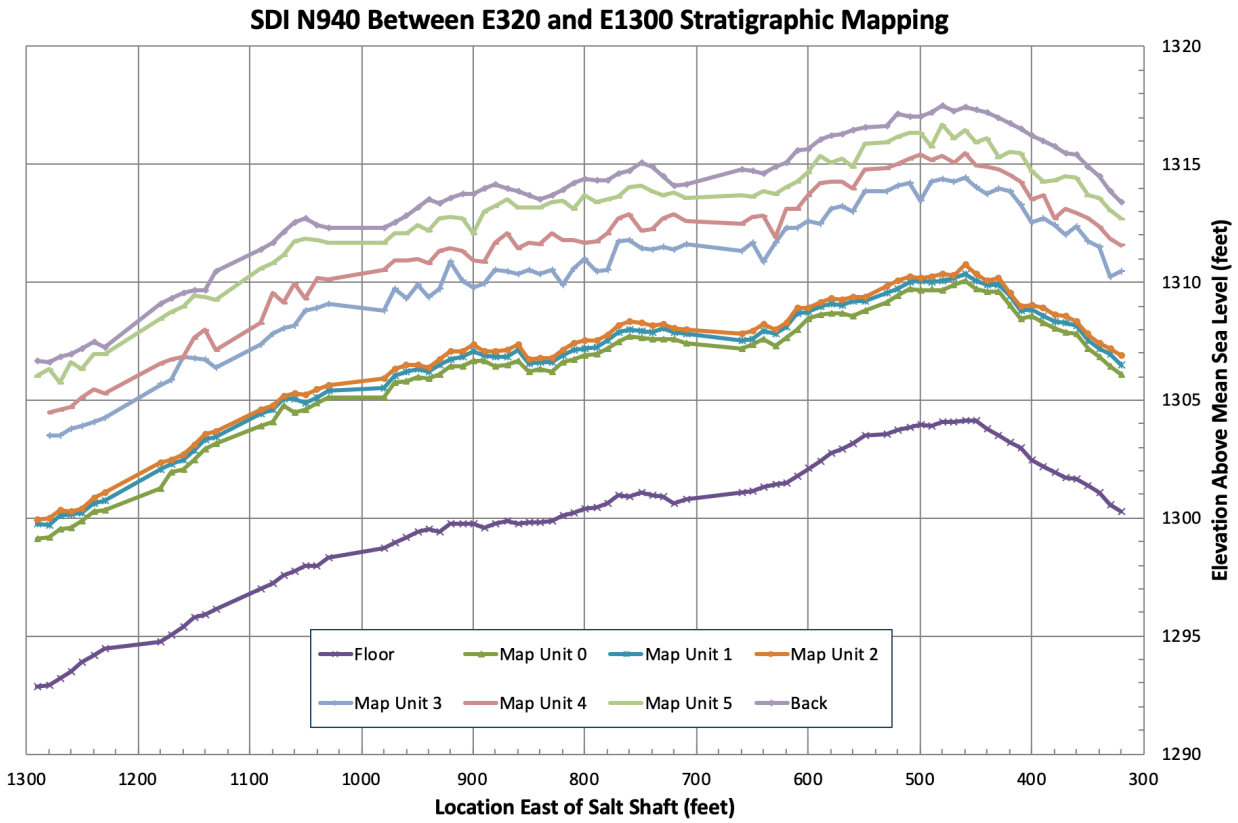

Figure 28. Survey data for tops of map units in E-940 (2013 survey by Wayne Stensrud, NWP)

Table 6. Geologic descriptions of map units (by Wayne Stensrud, NWP)

Description and Notes
MU-0: Argillaceous halite, clay content decrease with depth
MU-1: Orange Marker Bed (OMB) - Halite, reddish orange
MU-2: Argillaceous halite seam above OMB
MU-3: Halite, grading pink to gray
MU-4: Argillaceous halite, grey, reddish brown
MU-5: Argillaceous halite, bluish grey, Clay F
MU-6: Halite, grading grey to pink

Table 7. Borehole as-built coordinates and dimensions

Borehole ID	Actual Depth (ft)	Drill Bit Size (in)	Azimuth (deg)	Azimuth Direction	Inclination (deg)	Incline Direction	Bottom of Hole X Deviation (in)	Bottom of Hole Y Deviation (in)	Collar Center Line X Coord. (in)	Collar Center Line Y Coord. (in)	Bottom Center Line X Coord. (in)	Bottom Center Line Y Coord. (in)
U:T1	18.00	1.75	0.6	west	0.4	down	2.4	1.4	-37.63	0.50	-35.26	-0.93
U:T2	18.00	1.75	0.8	west	0.0	down	3.2	0.1	-25.63	0.50	-22.45	0.45
U:AE1	9.00	2.10	0.3	west	0.1	up	0.5	0.2	-9.63	12.00	-9.15	12.18
U:F2	30.01	1.75	0.2	east	0.2	down	1.1	1.0	-10.13	0.25	-11.26	-0.70
U:E2	18.00	1.75	0.3	west	0.1	up	1.2	0.3	-9.88	-6.00	-8.70	-5.71
U:AE2	9.00	2.10	0.1	west	0.6	up	0.2	1.1	-10.25	-12.25	-10.01	-11.18
U:E1	18.00	1.75	0.4	west	0.4	down	1.4	1.5	0.00	14.75	1.43	13.29
U:D	15.00	2.10	0.7	west	0.3	down	2.1	1.0	0.53	8.00	2.67	6.95
U:HP	12.13	4.80	0.6	east	0.7	down	1.5	1.8	0.00	0.00	-1.54	-1.75
U:F1	18.08	1.75	0.0	east	0.2	down	0.0	0.6	0.50	-8.00	0.50	-8.61
U:SL	8.05	4.80	0.3	west	0.9	down	0.5	1.5	8.00	11.00	8.54	9.54
U:SM	15.02	2.10	0.1	east	0.1	down	0.4	0.2	8.00	-0.50	7.61	-0.67
U:E3	18.01	1.75	0.1	east	0.3	down	0.3	1.0	7.75	-14.00	7.42	-14.98
U:AE3	9.02	2.10	0.1	east	0.3	up	0.2	0.7	16.63	0.75	16.39	1.41
H:T1	18.00	1.75	0.0	east	0.2	down	0.1	0.9	-37.75	0.29	-37.81	-0.57
H:T2	18.02	1.75	0.2	west	0.3	down	0.9	1.0	-25.63	0.38	-24.74	-0.62
H:AE1	9.00	2.10	0.0	west	0.0	level	0.1	0.0	-10.43	11.63	-10.35	11.63
H:F2	30.02	1.75	0.6	west	0.1	up	3.6	0.5	-10.38	0.25	-6.75	0.73
H:E2	18.02	1.75	0.4	west	0.3	down	1.5	1.0	-10.13	-6.63	-8.67	-7.63
H:AE2	9.03	2.10	0.5	west	0.0	level	0.9	0.0	-10.00	-12.25	-9.14	-12.25
H:E1	18.00	1.75	0.2	west	0.3	down	0.6	1.1	0.19	14.65	0.84	13.51
H:D	15.00	2.10	0.4	west	0.1	down	1.2	0.5	0.28	7.88	1.47	7.43
H:HP	12.23	4.80	0.9	west	0.3	down	2.4	0.8	0.00	0.00	2.43	-0.80
H:F1	18.01	1.75	1.3	west	0.3	up	5.0	1.1	0.50	-6.50	5.50	-5.40
H:SL	8.08	4.80	0.4	west	0.1	down	0.7	0.2	8.50	12.51	9.17	12.27
H:SM	15.01	1.75	1.2	west	0.6	up	3.8	2.0	8.00	0.76	11.78	2.74
H:E3	18.02	1.75	0.1	west	0.2	up	0.4	0.6	7.75	-13.36	8.14	-12.75
H:AE3	9.03	2.10	0.7	west	0.6	up	1.3	1.2	17.00	0.50	18.29	1.69

Table 8. Brine inflow volumes in unheated array

	Date Sampled	Brine Collected (mL)	Days Since Drilled	Cumulative inflow (mL)	Normalized Cumulative inflow (mL/m^2)
U:E3	4/18/19	100	64	100	118.6
U:D	4/18/19	40	5	40	47.9
U:HP	4/18/19	400	69	400	303.1
U:SL	4/18/19	350	4	350	398.0
U:SM	4/18/19	0	13	0	0.0
U:E1	4/18/19	620	5	620	736.0
U:AE1	4/24/19	10	11	10	19.9
U:D	4/24/19	30	11	30	36.0
U:HP	4/24/19	30	75	30	22.7
U:SL	4/24/19	20	10	20	22.7
U:SM	4/24/19	0	19	0	0.0
U:AE1	5/6/19	1.5	23	11.5	22.9
U:D	5/6/19	1.5	23	31.5	37.7
U:HP	5/6/19	5	87	35	26.5
U:SL	5/6/19	120	22	140	159.2
U:SM	5/6/19	0	31	0	0.0
U:T1	5/22/19	474	83	474	562.7
U:T2	5/22/19	250	44	250	296.8
U:AE1	5/22/19	24	39	35.5	70.8
U:AE2	5/22/19	0	98	0	0.0
U:AE3	5/22/19	12	79	12	23.9
U:E1	5/22/19	401	39	401	476.0
U:E2	5/22/19	2	100	2	2.4
U:E3	5/22/19	65	98	65	77.1
U:F1	5/22/19	0	103	0	0.0
U:F2	5/22/19	10	44	10	7.1
U:D	5/22/19	41	39	72.5	86.9
U:HP	5/22/19	16	103	51	38.6
U:SM	5/22/19	0	47	0	0.0
U:D	6/24/19	2	72	74.5	89.3
U:HP	6/24/19	5	136	56	42.4
U:SL	6/24/19	53	71	193	219.5
U:SM	6/24/19	0	80	0	0.0
U:AE1	7/23/19	0	101	35.5	70.8
U:D	7/23/19	35	101	109.5	131.2
U:HP	7/23/19	3	165	59	44.7
U:SL	7/23/19	66	100	259	294.6
U:SM	7/23/19	11	109	11	15.6

Table 9. Brine inflow volumes in heated array

	Date Sampled	Brine Collected (mL)	Days Since Drilled	Cumulative inflow (mL)	Normalized Cumulative inflow (mL/m^2)
H:T1	4/18/19	180	49	180	213.7
H:T2	4/18/19	100	49	100	118.6
H:AE2	4/18/19	40	52	40	79.5
H:E2	4/18/19	75	52	75	88.9
H:HP	4/18/19	80	60	80	60.1
H:SM	4/18/19	0	56	0	0.0
H:E1	4/24/19	180	6	180	213.7
H:D	4/24/19	5	6	5	6.0
H:HP	4/24/19	10	66	10	7.5
H:SL	4/24/19	60	6	60	68.0
H:SM	4/24/19	5	62	5	6.0
H:D	5/6/19	50	18	55	65.9
H:HP	5/6/19	5	78	15	11.3
H:SL	5/6/19	2	18	62	70.3
H:SM	5/6/19	0	74	5	6.0
H:T1	5/22/19	40	83	40	47.5
H:T2	5/22/19	55	83	55	65.2
H:AE1	5/22/19	24	33	24	47.8
H:AE2	5/22/19	6	86	6	11.9
H:AE3	5/22/19	12	89	12	23.8
H:E1	5/22/19	260	34	440	522.3
H:E2	5/22/19	20	86	20	23.7
H:E3	5/22/19	32	90	32	37.9
H:F1	5/22/19	6	94	6	7.1
H:F2	5/22/19	254	86	254	180.9
H:D	5/22/19	18	34	73	87.5
H:HP	5/22/19	14	94	29	21.8
H:SL	5/22/19	8	34	70	79.3
H:SM	5/22/19	7	90	12	14.4
H:AE1	6/24/19	10	66	34	67.8
H:D	6/24/19	7	67	80	95.9
H:HP	6/24/19	9	127	38	28.6
H:SL	6/24/19	27	67	97	109.9
H:SM	6/24/19	0	123	12	14.4
H:AE1	7/23/19	5	95	39	77.7
H:D	7/23/19	2	96	82	98.3
H:HP	7/23/19	0	156	38	28.6
H:SL	7/23/19	18	96	115	130.3
H:SM	7/23/19	8	152	20	24.0

Table 10. Brine composition (g/L) from samples collected on April 18, 2019

	B	Ca^{++}	Total Fe	K^{+}	Li^{+}	Mg^{++}	Na^{+}	Cl^{-}	Br^{-}	$SO_4^{=}$
U:HP	1.12	0.284	0.015	16.2	0.016	27.2	78.2	191	5.06	21.1
U:SL	1.00	0.324	0.003	15.1	0.017	24.1	74.9	189	5.13	20.3
U:E1	0.968	0.277	0.002	15.2	0.013	24.9	76.5	190	5.13	20.1
U:E3	0.799	0.228	0.004	13.3	0.01	21.8	66.6	163	4.59	18.4
U:D	0.756	0.238	0.001	12.8	0.009	20.7	63.8	150	4.73	17.5
H:HP	1.33	0.275	0.002	21.7	0.013	35.2	103	180	5.04	20.1
H:AE2	0.173	0.104	0.005	5.58	ND	9.56	30.7	71.3	4.10	10.3
H:E2	0.706	0.225	0.005	12.0	0.009	20.8	60.1	169	4.93	19.4
H:T1	1.28	0.364	0.009	18.7	0.019	30.7	98.2	169	5.05	18.6
H:T2	0.797	0.236	0.004	13.5	0.01	21.5	67.8	164	4.95	17.6

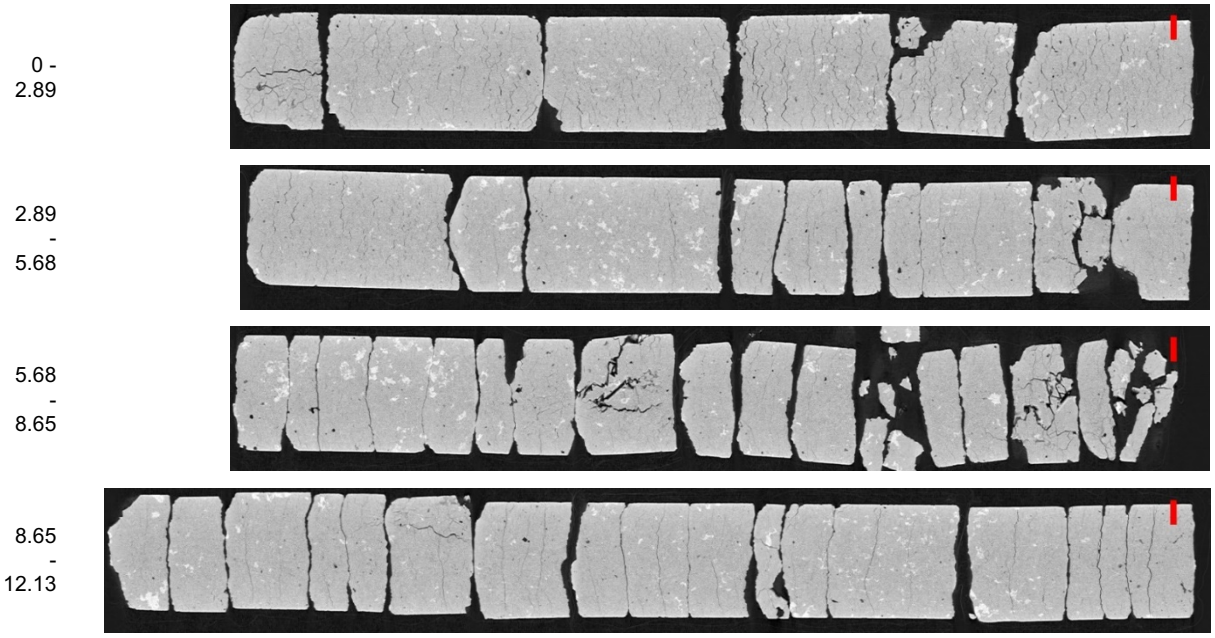

Figure 29. Preliminary X-ray CT scan results for SDI-BH-0006 (unheated HP). Scale bar 20 cm

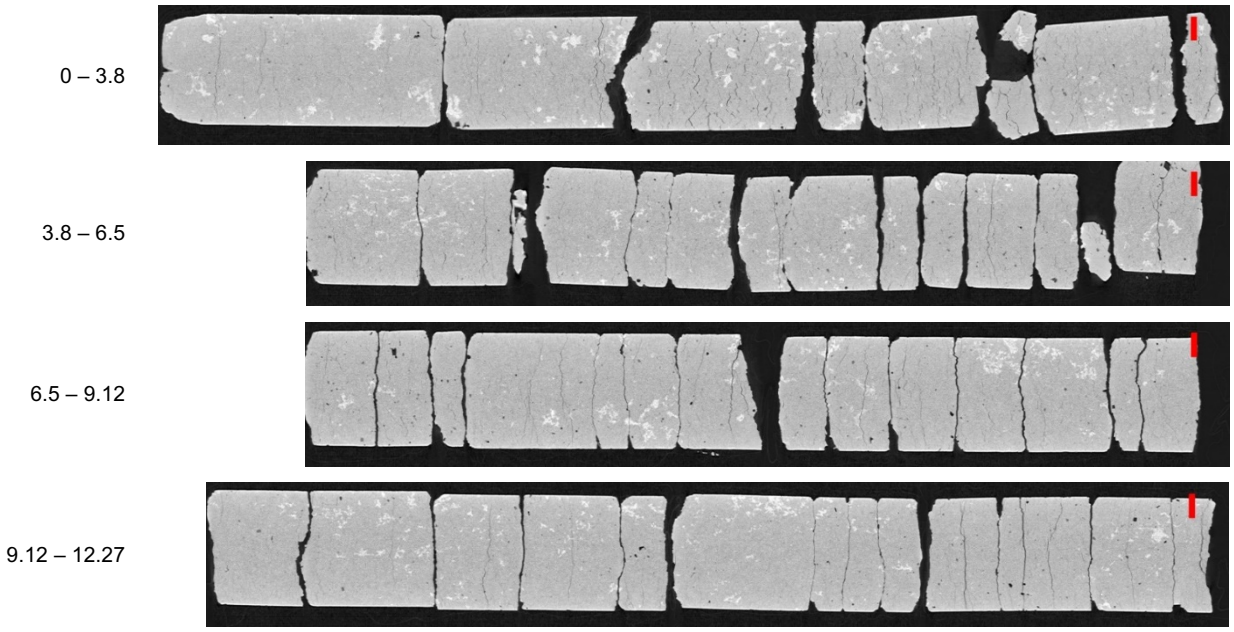

Figure 30. Preliminary X-ray CT scan results for SDI-BH-0007 (heated HP). Scale bar 20 cm

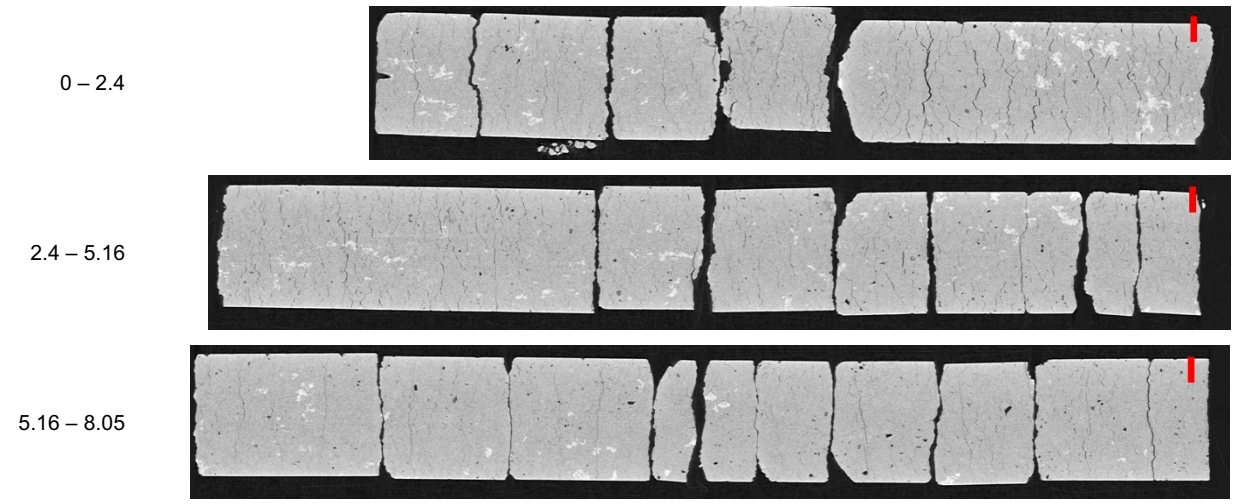

Figure 31. Preliminary X-ray CT scan results for SDI-BH-0008 (unheated SL). Scale bar 20 cm

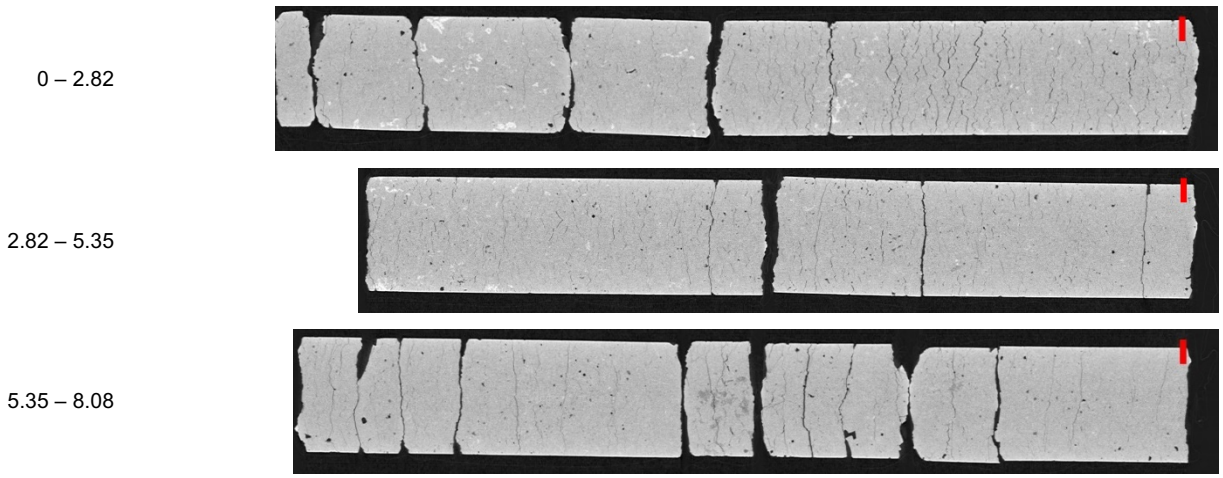

Figure 32. Preliminary X-ray CT scan results for SDI-BH-0009 (heated SL). Scale bar 20 cm

Table 11. Grouting measurements

Array	Borehole ID	Actual Depth [ft]	Borehole Diameter [ft]	Borehole Volume [in^3]	¾" PVC pipe volume* [in^3]	Date Grouted	Borehole Volume – PVC [L]	Used Grout Volume [L]	Difference [L]
Unheated	T1	18	0.16	625.4	78.5	5/23/19	8.96	6	-2.96
Unheated	T2	18	0.16	625.4	78.5	6/5/19	8.96	13	4.04
Unheated	F2	30.01	0.16	1042.7	130.8	6/5/19	14.94	16.5	1.56
Unheated	E1	18	0.16	625.4	78.5	6/5/19	8.96	10	1.04
Unheated	E1	18	0.16	625.4	78.5	6/5/19	8.96	10	1.04
Unheated	F1	18.08	0.16	628.2	78.8	6/5/19	9.00	8	-1.00
Unheated	E3	18.01	0.16	625.7	78.5	6/5/19	8.97	8	-0.97
Heated	T1	18	0.16	625.4	78.5	6/5/19	8.96	11	2.04
Heated	T2	18.02	0.16	626.1	78.5	6/5/19	8.97	10.5	1.53
Heated	F2	30.02	0.16	1043.0	130.9	6/5/19	14.95	17	2.05
Heated	E2	18.02	0.16	626.1	78.5	6/5/19	8.97	10	1.03
Heated	E1	18	0.16	625.4	78.5	6/5/19	8.96	10	1.04
Heated	F1	18.01	0.16	625.7	78.5	6/5/19	8.97	10.5	1.53
Heated	E3	18.02	0.16	626.1	78.5	6/5/19	8.97	10	1.03

*Volume of sensor wires and centralizers not included